THESIS FOR THE DEGREE OF DOCTOR OF PHILOSOPHY

Manganese ores as oxygen carriers for chemical-looping combustion

Sebastian Sundqvist

CHALMERS

Department of Chemistry and Chemical Engineering

CHALMERS UNIVERSITY OF TECHNOLOGY

Gothenburg, Sweden 2017

Manganese ores as oxygen carriers for chemical-looping combustion

Sebastian Sundqvist

ISBN: 978-91-7597-633-4

Doktorsavhandling vid Chalmers tekniska högskola.

Löpnummer: 4314

ISSN 0346-718X

Department of Chemistry and Chemical Engineering

Chalmers University of Technology

SE-412 96 Gothenburg

Sweden

Telephone +46 (0)31-772 1000

Cover:

Scanning electron microscope image from cross section of Tshipi manganese ore cast in epoxy.

Printed at Chalmers Reposervice

Gothenburg, Sweden 2017.

Manganese ores as oxygen carriers for chemical-looping combustion

Sebastian Sundqvist

Department of Chemistry and Chemical Engineering

Chalmers University of Technology

Abstract

Chemical looping combustion (CLC) is a fluidized bed system that circulates metal oxide particles in order to transport oxygen from an air reactor to a fuel reactor. In the fuel reactor a fuel reduces the oxygen carrier while producing CO_2 and H_2O. The oxygen carrier is then transported back to the air reactor and reoxidized. Chemical looping with oxygen uncoupling (CLOU) is similar to CLC, however the oxygen carrier differ as it has the ability to release gaseous oxygen in the fuel reactor. The advantage is that the oxygen released can react with the fuel directly, without the need for an intermediate gasification step.

Mainly oxide from Mn, Fe, Ni and Cu has been investigated as oxygen carrier. Of these, manganese oxides could be of interest for CLOU due to the ability to release O_2, especially when combined with other metals or metal oxides. Most of the investigated oxygen carriers are produced using various production methods, which could be costly. Another option is to use natural Mn-based minerals, such as manganese ores, which often contains the same elements as used to promote the CLOU effect, e.g. Fe, Si, Ca and Mg.

This thesis is a comprehensive study of manganese ore as oxygen carrier for CLC and CLOU. Here, twenty manganese ores have been investigated as potential oxygen carriers. They are evaluated with respect to reactivity with gaseous fuels CO/H_2 and CH_4 as well as their ability to release gaseous oxygen via oxygen uncoupling. Experiments were conducted with both batch and continuous CLC reactors.

From the experiments in this thesis it was found that all manganese ore release oxygen to varying degree, which suggests the presence of combined manganese oxides in the ores, something which was confirmed through particle and phase analysis. By utilizing solid char the extent and rates of oxygen release were determined for several ores at varying temperatures. It was found that most oxygen was released by Ca-rich ores, where up to 1 wt% oxygen could actually be released at higher temperatures.

The reactivity with fuel components and the mechanical stability varied depending on the ore utilized. Elemental mapping of individual particles indicate a significant inter-particle heterogeneity, while the intra-particle distribution was more even. Combination of XRD and SEM-EDX confirms a complex mineralogy with the presence of multiple phases which could be involved in CLC and CLOU, including $(Mn,Fe)_2O_3$, Mn_7SiO_{12} and $CaMnO_3$. The presence of these phases explains the CLOU effect that has been observed.

Keywords: Chemical-looping combustion, Chemical-looping with oxygen uncoupling, manganese ores, combined oxides, gaseous fuel, methane, syngas, wood char and solid fuels.

Acknowledgement

Here would like to express my gratitude to the people who made this work possible and who made this worthwhile.

First I would like to thank my main supervisor Associate Professor Tobias Mattisson. Thank you for your guidance, your time, your knowledge and your patience. I know we have had difficulties understanding each other at times but I very much like where we are now. Through working with you I have not only learned about research but also about myself and working with others. I have learned things that will benefit me where ever I will go, thank you.

Second I would like to thank my co-supervisor Professor Anders Lyngfelt. Thank you for your guidance, eye for details and critique. Thank you for all the work you did to obtain the ores, which I know was a struggle, and your enthusiasm toward manganese ores.

Third I would like to thank my second co-supervisor Associate Professor Henrik Leion. Thank you for your guidance, your knowledge and you general attitude. Thank you for lifting my spirit when times were the darkest.

Thank you to Dongmei, my friend and colleague. I know this will never reach your hands and I will always remember our conversations and arguments, the travels and the fun times. Thank you for providing me the opportunity to do my master thesis in China. Thank you and rest in peace

Thanks to my examiner and head of the division Professor Jan-Erik Svensson. Thank you for giving me the opportunity to go to China all those years ago and thank you for always taking time out of you fully packed schedule to see how things are going.

I would like to thank Tobias, Anders and Henrik for the opportunity to do my Ph.D. in field of CLC and in the group. I would like to thank the current and previous members of the CLC group Patrick, Matthias, Carl, Peter, Malin, Jesper, Magnus, Pavleta, Georg, Dazheng, Mehdi, Golnar, Volkmar, Martin. Thank you for all your help, it has been a pleasure of working with you.

Thanks to my two office mates Jan and Patrick it has been fun sharing an office with both of you. Thank you everyone in the division of inorganic environmental chemistry. Thanks to my student Nazli, it was a pleasure working with you. Thank you to all the guest researchers and master students that I had the pleasure of meeting. Despite the hardships if I had to do it all over again I would do it if only to meet all of you.

Last but not least I would like to thank my family who always supported me. Always give me space when I need it, always ready to listen and help. Thank you.

Sebastian Sundqvist

Gothenburg, August 31, 2017.

List of publications

The thesis is based on the work presented in the following papers.

Paper I

Sundqvist, S.; Leion, H.; Rydén, M.; Lyngfelt, A., $CaMn_{0.875}$ $Ti_{0.125}O_{3-\delta}$ as an Oxygen Carrier for Chemical-Looping with Oxygen Uncoupling (CLOU)—Solid-Fuel Testing and Sulfur Interaction. *Energy Technol*. 2013; 1(5-6): 338-344.

Paper II

Sundqvist, S.; Arjmand, M.; Mattisson, T.; Rydén, M.; Lyngfelt, A., Screening of different manganese ores for chemical-looping combustion (CLC) and chemical-looping with oxygen uncoupling (CLOU). *Int J Greenh Gas Control*. 2015; 43: 179-188.

Paper III

Sundqvist, S.; Khalilian, N.; Leion, H.; Mattisson, T., Manganese ores as oxygen carriers for chemical-looping combustion (CLC) and chemical-looping with oxygen uncoupling (CLOU). *J Environ Chem Eng*. 2017; 5 (3): 2552-2563

Paper IV

Sundqvist, S.; Mattisson, T.; Leion, H.; Lyngfelt, A., The use of manganese ore for chemical-looping with oxygen uncoupling. Submitted for publication.

Paper V

Moldenhauer, P.; Sundqvist, S.; Mattisson, T.; Linderholm, C., Chemical-looping combustion of synthetic biomass volatiles with manganese-ore oxygen carriers. Submitted for publication.

Paper VI

Sundqvist, S.; Moldenhauer, P.; Leion, H.; Lyngfelt, A.; Mattisson, T., Influence of heat treatment on manganese ores as oxygen carriers. In manuscript.

Contribution report

I. First author, responsible for experimental work, data evaluation and writing.

II. First author, responsible for experimental work, data evaluation and writing.

III. First author, responsible for part of the experimental work, responsible for data evaluation and writing.

IV. First author, responsible for experimental work, data evaluation and writing.

V. Second author, responsible for part of the experimental work, shared responsibility for data evaluation and writing.

VI. First author, responsible for experimental work, data evaluation and writing.

Related papers not included in the thesis

Schwebel, G. L.; Sundqvist, S.; Krumm, W.; Leion, H., Apparent kinetics derived from fluidized bed experiments for Norwegian ilmenite as oxygen carrier. *Journal of environmental engineering.* 2014; 2: 1131-1141.

Schmitz, M.; Linderholm, C.; Hallberg, P.; Sundqvist, S.; Lyngfelt, A., Chemical-looping combustion of solid fuels using manganese ores as oxygen carriers. *Energy Fuels.* 2016; 30: 1204-1216.

Table of Contents

1 Introduction

1.1 Global warming

The global surface temperature of the Earth has been rising during the last decades[1]. The rapidly rising temperature is affecting the climate in several ways, including melting glaciers and a rise in sea level. The change in climate is attributed to the increased amount of greenhouse gases in the atmosphere, which traps infrared radiation leading to increased global temperature[2]. The gases that are considered greenhouse gases are mainly fluorinated gases, nitrous oxides (N_2O), methane (CH_4), and carbon dioxide (CO_2)[1]. The latter is considered the most important anthropogenic greenhouse gas, which can be attributed to the significant quantities being emitted to the atmosphere today.

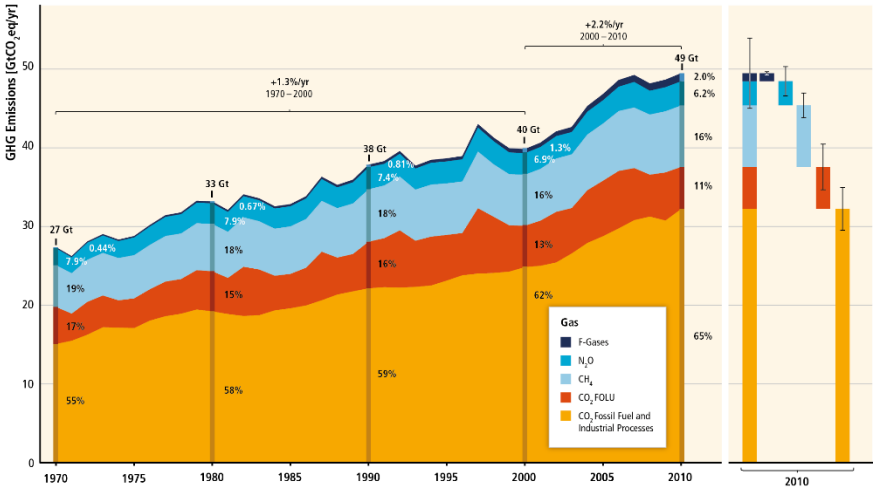

Figure 1: Total annual anthropogenic greenhouse gas emissions by groups of gases 1970–2010[1]

In Figure 1 it can be seen how the greenhouse gas emissions have been rising during the last 40 years[1]. 2% of the total emissions of greenhouse gases, normalized to CO_2 equivalent, are fluorinated gases emitted from industries and refrigeration, which includes both residential buildings and vehicles. Nitrous oxides and methane, 6% respectively 16% of the total emissions, are released during agriculture activities and combustion of biomass. Nitrous oxides are released through the use of fertilizer for soil enrichment while methane is released from enteric fermentation in livestock and from manure management. The largest part of the greenhouse gas emissions is again carbon dioxide, which accounts for 76% of the total emissions and is released through land clearing for agriculture, deforestation and combustion of fossil fuels[1,3]. With respect to the latter, the main sectors contributing to the CO_2 emissions are industry, electricity generation, and transportation, each contributing about 1/3 to the total emissions of carbon dioxide.

Given the dominance of fossil fuels and that there is an ever increasing demand for energy, measures need to be taken to stabilize CO_2 levels. Some such measures are improving efficiency of both power generation and energy utilization, increasing reliance on wind, solar and nuclear power[3,4]. However, while these measures will most likely be important, it is unlikely that they will be enough to achieve the necessary reductions. An additional option is carbon capture and storage, the main topic of this thesis.

1.2 Carbon Capture and Storage (CCS)

One proposed strategy to significantly reduce greenhouse gas emissions rapidly is to use carbon capture and storage (CCS). Here,CO_2 from large point sources, such as power plants is captured, compressed and stored in geological formations such as depleted oil and gas fields[5,6] or saline aquifers[7]. It is important that the carbon dioxide is stored for thousands of years[1] to enable biospheric processes to equilibrate and remove carbon from the atmosphere, e.g. removal by oceans or weathering. However, as mentioned earlier, greenhouse gases consist of more than just CO_2. Hence, even if CCS is implemented at large scale it cannot inhibit all emissions of greenhouse gases. This means that CCS will be part of a portfolio of technologies needed in order to achieve sustainability. Most of the CO_2 emitted during electricity generation can be captured, and possibly a large part of industrial emissions as well[4]. The current fossil fuel based transportation sector is not directly applicable for CCS, as the emissions are small and disperse. However, if the transportation system was changed to be electricity based then emissions could be shifted to point sources, e.g. power plants, which would make CCS much easier.

Another interesting option to reduce greenhouse gas emissions is the implementation of bio-energy with carbon capture and storage (BECCS)[8]. In BECCS, biomass-based fuels are used for heat and power generation, which would enable capturing CO_2 that was absorbed by plants during growth. This would result in “negative emissions” of carbon dioxide, i.e. a net flow of carbon out of the atmosphere into the ground. It is thus possible to actually reduce the atmospheric concentration of carbon dioxide using BECCS, provided that biomass is regrown in a sustainable way. With no binding climate agreements in place, negative emissions will likely be needed at large scale in the future, if we are to stabilize the temperature rise to below 2˚C. Several techno-economic models have shown that climate goals can be achieved at lower cost if BECCS is included in the energy portfolio, e.g. Azar et al.[8,9] Further, a recent major study identifies CCS and bioenergy as the two most valuable technologies for achieving climate policy objectives (more important than energy efficiency improvements, nuclear power, solar power and wind power), motivated by their combined ability to produce very significant negative emissions via BECCS[10].

Once CO_2 has been captured it needs to be stored for a significant time period. In order to store the CO_2, it needs to be compressed to a liquid and transported to the storage site. Both of these activities are associated with an energy penalty and cost[11,12]. Most of the storage capacity can be found off-shore[11,12] in form of aquifers. Some storage capacity is found on-shore or inland, but political issues may prevent them from being used. This means that off-shore storage is the most

likely option to be utilized. The transport to the storage sites can be done with ships or pipelines, depending on the volume of CO_2 that needs to be transported[11,12]. If there are many smaller capture points close to the coastline then transport by ship is preferable, while larger emission sources could warrant the construction of a pipeline[11,12]. However small emission sources that are not located close to the coastline presents a problem; they are unreachable with ship and a pipeline is often not economically feasible[11,12].

1.3 CO_2 Capture Technologies

This thesis is related to the capture of carbon dioxide, and thus the main technologies will be discussed briefly. CO_2 capture technologies are usually divided into three groups: Pre-combustion, post-combustion and oxyfuel[4].

The first process, pre-combustion is a method, where the fuel is first gasified into a syngas, a mixture of CO and H_2, with either O_2 or steam. After that, CO is converted into CO_2 with steam through the water-gas shift reaction. The CO_2 is then separated from the hydrogen with a chemical or physical absorbent. Such absorption processes are commercially available. The drawback, however, is the energy required for gas separation [13].

In the post-combustion process the CO_2 separation occurs after conventional air combustion. The CO_2 in the flue gas is separated from N_2, O_2, NO_x, SO_x and any other gases in the flue gases, for example through adsorption, absorption or membrane separation[14]. There are other processes that utilize solid materials in order to adsorb or react with the CO_2 in the flue gas stream, such as calcium looping[15]. The benefit of post-combustion is that the process in theory could be added to existing power plants. In practice, however, retrofitting create difficulties such as heat integration and placement of capture equipment. Post combustion has significant energy requirements, as a rather low concentration of carbon dioxide in the gases from the combustion chamber needs to be separated from the rest of the flue gases.

The last of the three groups is oxyfuel combustion, where instead of air, oxygen mixed with recycled flue gases is used as oxidizing agent[16]. Ideally this leads to a pure flue gas stream of CO_2 and H_2O in the form of steam. The steam can easily be removed through condensation. However, the process still requires O_2 to be separated from the air, which is associated with a significant energy input[17].

All these three methods entail some type of gas separation step, which require not only significant amounts of energy, but also equipment in order to implement the separation. The fourth type of carbon capture technology is chemical-looping combustion (CLC), the main topic of this thesis. CLC is a form of unmixed combustion where carbon dioxide is inherently obtained in pure form, without the need for gas separation. Below follows a more detailed description of this technology.

1.4 Chemical-Looping Combustion

A method for carbon capture from the combustion of fuels with inherent separation of CO_2 is available in chemical-looping combustion (CLC). In this form of unmixed combustion there is no active gas separation and hence, no direct energy penalty, which is generally required in other carbon capture processes [18]. A CLC system consists of two interconnected fluidized bed reactors, one air reactor and one fuel reactor, illustrated in Figure 2. Oxygen is transported from the air reactor to the fuel reactor through the oxidation of a metal oxide (Me_xO_y), an oxygen carrier, which is circulated to the fuel reactor, where the oxygen carrier reacts with the fuel [19]. After the oxygen carrier has been reduced it is transported back to the air reactor to be oxidized again.

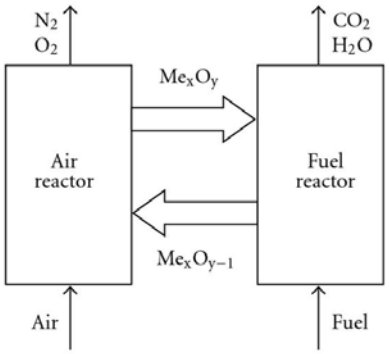

Figure 2: Schematic representation of the CLC process.

It is possible to employ gaseous, liquid and solid fuels in a chemical looping process[20–23]. The gaseous fuels such as methane and intermediates such CO and H_2 reacts directly with the oxygen carrier as in the overall reactions (Re. 1)-(Re. 3).

$$Me_xO_y + CH_4 \rightarrow Me_xO_{y-1} + CO_2 + 2H_2O \qquad \textit{(Re. 1)}$$

$$CO + Me_xO_y \rightarrow CO_2 + Me_xO_{y-1} \qquad \textit{(Re. 2)}$$

$$H_2 + Me_xO_y \rightarrow H_2O + Me_xO_{y-1} \qquad \textit{(Re. 3)}$$

In order to achieve reasonable reaction rates between the oxygen carrier and fuel, the latter needs to be in a gaseous form, as given in the above equations. Hence, for natural gas, containing mostly methane, the fuel will react directly through overall reaction (Re. 1). For solid fuels, the reaction path is a little more complicated. The fuel will rapidly devolatilize in the fuel reactor to char and volatile components. The volatiles will react directly with the oxygen carrier particles. As the solid char likely will not react with the oxygen carrier at any appreciable rate, it needs to be transferred to a gas. Hence, there is need for gasification of the solid fuel, which is done with either H_2O or CO_2 according (Re. 4) and (Re. 5) to produce the reactive components H_2/CO, which can then react

with the oxygen carrier. The entire sequence of reactions, i.e. gasification and oxidation, can be carried out in one reactor vessel, i.e. the fuel reactor[19,21].

$$C + H_2O \rightarrow CO + H_2 \qquad \textit{(Re. 4)}$$

$$CO_2 + C \rightarrow 2CO \qquad \textit{(Re. 5)}$$

Ideally the outlet gases from the fuel reactor consists only of CO_2 and steam. The steam is removed through cooling and condensing of water, which results in a gas stream that ideally consists of pure CO_2.

Once the oxygen carrier has been reduced in the fuel reactor it is transported back to the air reactor, where it is once again oxidized according to (Re. 6). The overall reaction has the same heat production as conventional combustion.

$$2Me_xO_{y-1} + O_2 \rightarrow 2Me_xO_y \qquad \textit{(Re. 6)}$$

Another possibility for conversion of solid fuels is a process known as chemical looping with oxygen uncoupling (CLOU). In this process the oxygen carriers releases oxygen according to (Re. 7). The extent and rate depends on the partial pressure of oxygen during oxidation, the thermodynamics of the oxygen carrier and the conditions in the fuel reactor[24]. The oxygen then reacts with the fuel through normal combustion as shown in (Re. 8)[19,21,24]. The oxygen carrier is then transported back to the air reactor where it is reoxidized according to (Re. 6), i.e. the same overall step as for CLC. The overall enthalpy of CLOU also has the same heat production as conventional combustion.

$$2Me_xO_y \rightarrow 2Me_xO_{y-1} + O_2 \qquad \textit{(Re. 7)}$$

$$C_nH_{2m} + \left(n + \frac{m}{2}\right) O_2 \rightarrow nCO_2 + mH_2O \qquad \textit{(Re. 8)}$$

The main advantages with a CLOU reaction, is that the relatively slow gasification reactions, i.e. (Re. 4) and (Re. 5) will be totally or partially eliminated, and “replaced” with combustion, yielding a higher rate of char conversion. It could also be expected that CLOU could have significant advantages also with gaseous[25,26] and liquid fuels[27,28]. Depending upon the kinetics of oxygen release, a CLOU reaction in the fuel reactor may be accompanied by a parallel CLC reaction, i.e. part of the fuel will be oxidized by gas-phase oxygen while other parts will react with the oxygen carrier directly. The influence of CLOU and CLC reactions may vary for different operational conditions and different oxygen carrier materials[29].

1.4.1 Oxygen Carriers

The oxygen carrier is a metal oxide and the properties of the oxygen carrier is largely dependent on what metal oxide it consists of. The oxygen carrier needs to have high reactivity with fuel, high resistance towards attrition, low environmental impact, be non-toxic, and have a low cost. In order for a metal oxide system to be considered as an oxygen carrier for CLOU, it is required to have a high equilibrium of O_2 in the temperature range (800-1000˚C). This is so that there can be a transition between two oxidized phases, which results in a release of oxygen as a more oxidized phase decomposes, see (Re. 7).

A significant number of oxygen carrier materials have been investigated during the last two decades[21,30,31]. Research has focused on the systems Fe_2O_3/Fe_3O_4, NiO/Ni, CuO/Cu, Co_3O_4/CoO, and Mn_3O_4/MnO[21,32–38]. These systems have a high thermodynamic propensity to convert hydrocarbon fuels to carbon dioxide and water at combustion temperatures. Normally, various types of supports, such as Al_2O_3 and SiO_2, are used together with the active material, but also natural ores and minerals have been employed. Today, thousands of oxygen carrier materials have been investigated in the literature, and reviews of the performance can be found in a number of review papers. A complete review is beyond the scope of this thesis, but a general comparison of reactivity, cost and environmental safety and health risk of the main oxygen carrier materials can be found in Table 1. Both NiO/Ni and Co_3O_4/CoO have high reactivity but are toxic as well as having a high cost. CuO/Cu also has high reactivity and high price. The drawback is the low melting point (1085˚C) of metallic Cu, which could result in agglomeration/defluidiztion in a fluidized bed. Another important aspect is the thermodynamics, which will be discussed below in Section 1.4.2. It should be noted that lately there have been a lot of focus on CLOU materials, these systems will also be discussed in the next section.

Table 1: Comparison of reactivity, cost and environmental safety and health of the monometallic oxygen carrier materials.

	Fe_2O_3/Fe_3O_4	Mn_3O_4/MnO	CuO/Cu	NiO/Ni	Co_3O_4/CoO
Reactivity	1	2	3	3	3
Cost	1	2	3	3	3
Environmental and health risk	1	1	1	3	3
Thermodynamic yield of fuel to CO_2 and H_2O	3	3	3	2	2

1=low, 2=medium, 3=high.

1.4.2 Thermodynamics of oxygen carriers

Jerndal et al.[32] conducted a comprehensive investigation of a large number of oxygen carrier systems for CLC. Several systems were identified as having high propensity to convert hydrocarbon fuels to CO_2 and H_2O, see Table 1. In the same study, several oxide systems were found to spontaneously decompose at high temperatures, and thus deemed not to be suitable for CLC. This included the phases CuO/Cu_2O, Co_3O_4/CoO and Mn_2O_3/Mn_3O_4. Figure 3 shows the partial pressure of O_2 for some of these systems. It can be observed that the partial pressure of oxygen is considerable at combustion temperatures, meaning that the most oxidized phases will spontaneously decompose in the fuel reactor. Mattisson et al. however proposed to use the decomposition as a possible advantage and suggested to use the decoupled oxygen for combustion, thus proposing the concept chemical-looping with oxygen uncoupling (CLOU)[24,39]. The equilibrium temperatures of Fe_2O_3/Fe_3O_4, Mn_3O_4/Mn_2O_3, MnO_2/Mn_2O_3 and CuO/Cu_2O can be seen in Figure 3. The phase transition of Fe_2O_3/Fe_3O_4 occurs at even higher temperature, 1300˚C at pO_2=0.05, which means that Fe_2O_3 decomposes above this temperature. This temperature is generally too high for normal fluidized bed combustion systems and makes Fe_2O_3/Fe_3O_4 unsuitable for CLOU. CuO/Cu_2O is of interest as it has shown to rapidly release oxygen in the temperature range 850-950˚C. For MnO_2/Mn_2O_3 the transition at pO_2=0.1 occurs at 400˚C and Mn_3O_4/Mn_2O_3 at around 800˚C, which means that it can take up oxygen below those temperatures[24]. Reactivity at these temperatures is likely to low[40] to be useful for these types of systems.

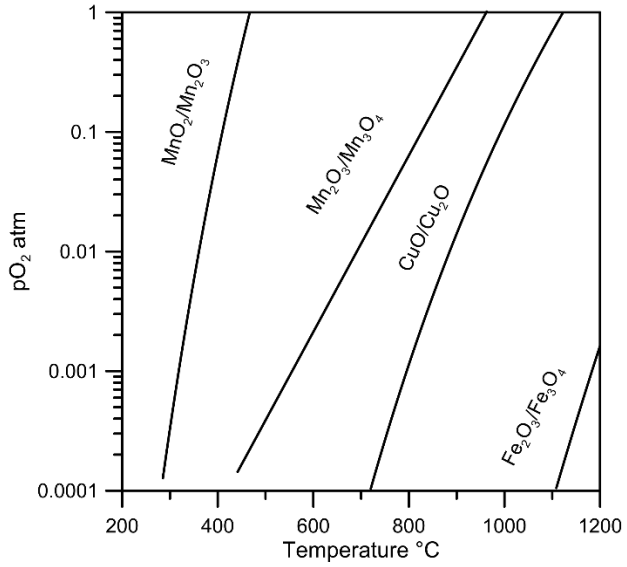

Figure 3: Phase diagram of some relevant manganese, copper and iron oxides. The diagram was constructed using Factsage 7.0 with FToxid database.

The relevant phase transition temperatures for pure Mn-based oxides in Figure 3 are likely too low for use in CLOU, and all experimental data point towards slow kinetics of oxidation of Mn_3O_4[40]. However, in 2009 Shulman et al.[41] found that by combining Mn_3O_4 with Fe, Si and Ni, significant uncoupling rates could be obtained. Since then a number if such combined systems have been investigated. e.g. Mn-Fe-O[42], Mn-Fe-Al-O[43], Mn-Si-O[44]. The superior behavior can in many cases

be explained by altered thermodynamics in comparison to the monometallic and pure system. For instance, Figure 4 shows the phase diagram for the Mn-Fe-O binary at an O_2 partial pressure of 0.05 atm, highly relevant for CLOU[42]. A combined metal oxide with a ratio of Mn/(Mn+Fe) = 0.8 would have phase transitions around 900˚C. If the Fe content is increased the transition temperature for full transitions between $(Mn,Fe)_2O_3$ and $(Mn,Fe)_3O_4$ increases making the oxygen carrier suitable at combustion temperatures, where reactivity is expected to be sufficiently high.

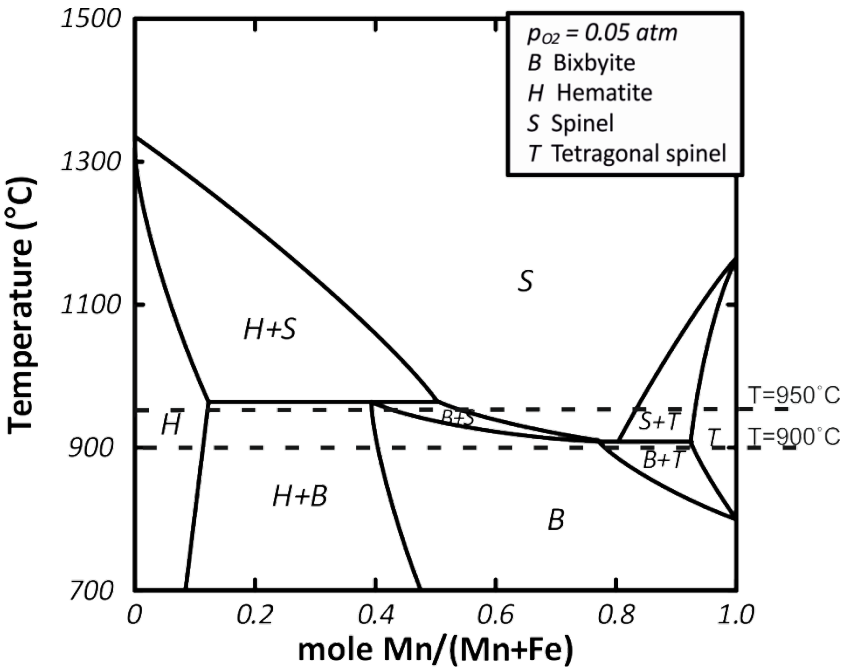

Figure 4: Phase diagram of Mn-Fe binary oxide system at O_2 partial pressure of 0.05 atm[42].

Another possibility is to use a combined oxide of Mn and Si. Figure 5 shows a phase diagram of the Mn-Si system at an O_2 partial pressure of 0.05 atm[45]. The content of Si is limited to 15 mole% in order to have the phase transition below 1000˚C. Some of the possible manganese silicates are braunite (Mn_7SiO_{12}), rhodonite ($MnSiO_3$) and tephroite (Mn_2SiO_4). When temperature is increased braunite and tridymite reacts to form rhodonite which releases O_2.

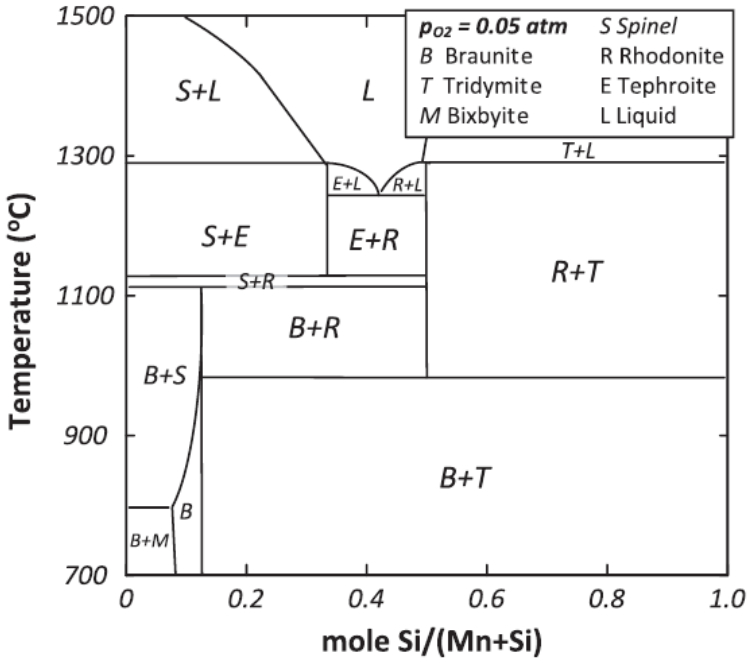

Figure 5: Phase diagram of Mn-Si binary oxide system at O_2 partial pressure of 0.05 atm[45].

Another promising combined oxygen carrier consists of Ca and Mn forming $CaMnO_{3-\delta}$, a perovskite-type material with the general formula $ABO_{3-\delta}$. For this type of material, the oxygen deficiency (δ) varies depending on the partial pressure of oxygen and temperature[46]. When the partial pressure of O_2 decreases, the deficiency increases as the material releases oxygen according to (Re. 9).

$$2ABO_{3-\delta} \rightarrow 2ABO_{3-\delta-a} + aO_2 \qquad \textit{(Re. 9)}$$

In contrast to the previous two binary oxide systems, $CaMnO_{3-\delta}$ doesn't have a distinct phase transition between $ABO_{3-\delta}$ and $ABO_{3-\delta-a}$ but rather a gradual transition, which again depends upon the degree of oxygen deficiency. The benefit of the gradual transition is that there is no phase change hence less structural change which increases the mechanical stability through reduced stress on the particles. The thermodynamics of the most common material $CaMnO_3$ has been explored previously[47–49].

1.4.3 Manganese-based oxygen carriers

There has been a significant amount of research on synthetic manganese oxygen carriers, especially combined metal oxides, which can release oxygen to the gas phase, and in this way improve fuel conversion. These studies are summarized in Figure 6, in forms of ternary triangles. Extensive investigations have been done with respect to the Fe-Mn system, including investigations of the effect of composition, fuel and support material[42,43,50,51]. In a study by Azimi

et al. it was found that oxygen carriers with a Mn content between 20 wt% and 40 wt% release oxygen[42]. Shulman et at. investigate several combinations of Mn-Si and Mn-Mg[41,52] and found that both of the combined materials release oxygen and can be reoxidized at 900˚C, which was not possible for the pure Mn system. Jing et al. conducted a comprehensive investigation of the Mn-Si system[53], which showed that the highest reactivity and the highest amount of oxygen released were obtained from an oxygen carrier with 25 wt% SiO_2 and the rest Mn_3O_4. Frick et al investigated oxygen carriers based on Mn-Si-Ti[44], where the Ti was used to mechanically stabilize the particles. It was found that the Mn-Si-Ti oxygen carriers have a high reactivity towards methane and a high resistance to attrition. Arjmand et al. studied the Mn-Fe-Si system[54] and found that the oxygen carriers had significant oxygen release and high reactivity towards syngas (50/50, H_2/CO). Källén et al. investigated Mn-Si and Mn-Si-Ti in a 300W continuously circulating unit[26] and found that Mn-Si had higher reactivity but lower attrition resistance than Mn-Si-Ti.

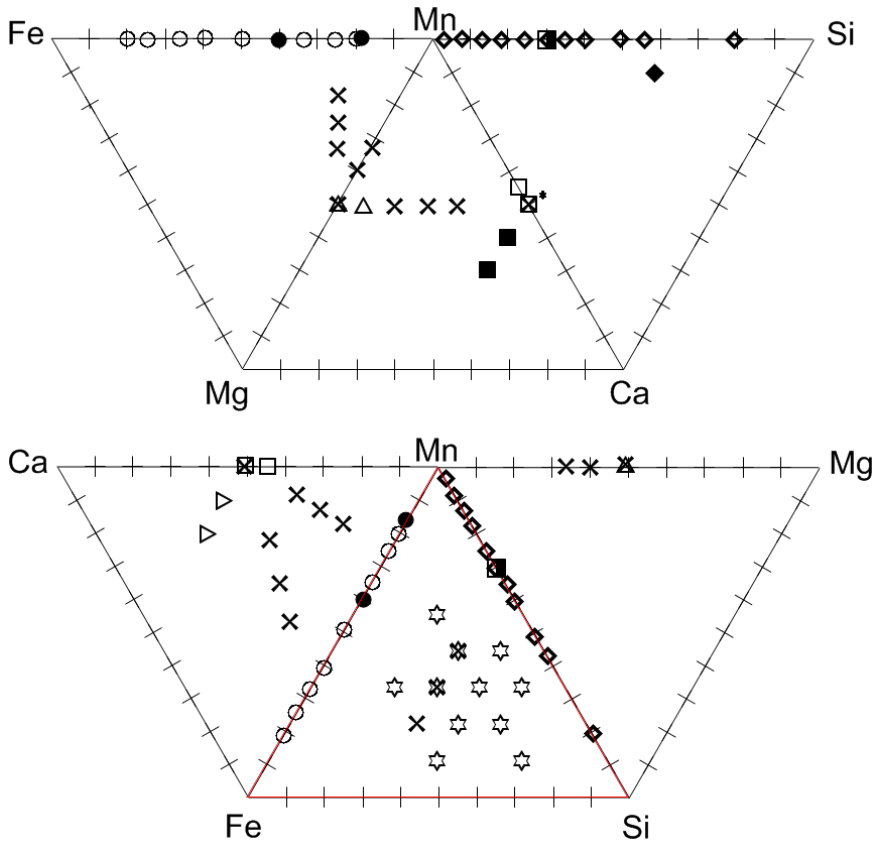

*Figure 6: Molar fractions of metals/metalloids of investigated combined manganese oxides. Symbols indicate compositions which have been investigated in the literature according to Mattisson et al.,[55](✕), Azimi et al., [42](○), Shulman et al., [41](●), Shulman et al., [52](△), Jing et al., [53](◇), Frick et al., [44](◆), Arjmand et al., [56](□), Jing et al., [57](■), Hallberg et al., [25](▷), Arjmand et al., [54](✡). *Several works have studied particles in the Ca-Mn binary with a similar amount of Ca and Mn, often doped with additional metals, e.g.* [58–60]

The Mn-Ca system is especially interesting since the perovskite-structured $CaMnO_3$ has very prominent oxygen-release properties[61–63]. Calcium manganite-based oxygen carriers yielded promising results in a batch reactor, a 300 W unit and a 10 kW unit[61–65]. It was found that the $CaMnO_3$ particles achieved a high conversion of fuel and the reactivity showed no sign of deterioration after 99 h of continuous operation with fuel using a 10 kW pilot[65]. This type of perovskite has clearly been one of the more promising materials, and was studied in two major EU-financed projects, i.e. INNOCUOUS (2010-2013) and SUCCESS (2013-2017). The main problem with this type of oxygen carrier is the possible deactivation with sulphur, something which was first noted in Paper I of this thesis. Here, it was found, that when exposed to sulphur, the perovskite phase $CaMn_{0.875}Ti_{0.125}O_{3-\delta}$ decomposed and $CaSO_4$ was formed, leading to a loss in reactivity. The amount of $CaSO_4$ that formed was proportional to the amount of SO_2 that was introduced to the system. Several later studies could confirm this effect, although the chemistry is not entirely understood[56,59]. This vulnerability to Sulphur makes this material an unlikely candidate for any sulphurous fuels, e.g. coal or sulphurous natural gas, the latter which would have to be desulphurized before use.

However manganese is still of great interest and there is the option of lowering cost by using manganese-based minerals, i.e. ores. It is not uncommon that manganese ore contains many of the components previously investigated such as Fe, Ca, Si and Mg. This opens up the possibility of good yet cheap oxygen carrier with potential to possess some of the interesting active phases discussed above such as $CaMnO_3$, Mn-Fe-Si, Mn-Fe-Ti.

1.4.4 Naturally occurring manganese oxygen carriers

When this work began there was little research done on manganese ores as oxygen carriers for chemical looping[66]. During the last couple years a number of publications have been published that deal with manganese ores in CLC, including the work presented in this thesis. However, most of the research has been focused on phase composition, catalysis and reaction kinetics, and not specifically on the evaluation of the CLOU effect, which is one of the key focuses in this thesis[67–70].

Combined oxide oxygen carriers have been produced using manganese ores as starting material. These studies have focused on evaluating oxygen carriers that were produced from manganese ores mixed with CaO or $Ca(OH)_2$ in order to produce particles that contain the perovskite phase $CaMnO_{3-\delta}$[66,71]. In one of these investigations, the ores were analyzed with both X-ray diffraction (XRD) and in a TGA to determine the phases that had formed, the oxygen carrying capacity as well as the release of oxygen from the particles[66]. It was found that the particles had an oxygen capacity of 4.9 wt% at 1000 ˚C and that the perovskite phase had formed[66]. In another investigation, the particles were studied using a batch fluidized system[71]. The ore-based oxygen carriers were compared with oxygen carrier produced from synthetic raw materials. It was found that the ore-based oxygen carriers had higher attrition resistance but lower reactivity than the synthetic ones[71].

Modified manganese particles were studied by Xu et al. where manganese ores were impregnated with a copper nitrate solution attempting to enhance the reactivity of the oxygen carrier[72,73]. The copper impregnated manganese ore were compared to unmodified manganese ore in a fluidized bed reactor. It was found that the reactivity was significantly enhanced by the impregnation with copper[72,73].

Manganese ores as oxygen carriers have also been investigated in batch fluidized systems. Poor mechanical stability of manganese ore was found by Leion et al.[74] Here, poor fluidization properties were also seen when comparing manganese ore with refined manganese materials, such as color pigment. Arjmand et al.[70] investigated how the presence of manganese ore affects the rate of steam gasification of petcoke. It was found that the rate of gasification increases with manganese compared to ilmenite. The effect was speculated to be because of oxygen release, suppression of H_2 inhibition and possible catalytic effects. This was further investigated by Frohn et al[75], and it was concluded that the suppression of the H_2 inhibition was not the main reason for the increase in gasification rate. Keller et al[69], determined that the potassium in the ore catalyzed the steam-carbon gasification reaction. In a follow-up investigation, Arjmand et al.[76] found that the rate of char gasification was correlated to the concentration of potassium and sodium in the manganese ore.

Manganese ores have also been investigated in continuous operation, including tests in a 300 W reactor using natural gas[77] and a 10 kW CLC reactor using solid fuel[78]. In the 300 W circulating fluidized bed system Rydén et al[77] compared a manganese ore with a particle produced from 66.8 wt% iron oxide and 33.2 wt% manganese oxide. It was found that the synthetic particle has higher oxygen release than the manganese ore at 1000°C and that oxygen release increased with temperature. The oxygen release experiments were performed using CO_2 to fluidize the bed, and this could be maintained for 8 h. However when the experiment used natural gas as a fuel the experiment had to be discontinued after a few hours due to collapse of the particles.

Schmitz et al. investigated the performance of several manganese ores using a 10 kW CLC reactor[78] with wood char and petcoke as fuel. The ores were evaluated during continuous operation with regards to the effect on the gas conversion, carbon capture efficiency and lifetime of the oxygen carrier. It was found that manganese ores could be used successfully in continuous operation with high carbon capture efficiencies (>90%). Some ores formed agglomerates and were discarded as potential oxygen carriers, but of those that did not form agglomerates, lifetimes of up to 284 h were estimated based on production of fines[78]. A manganese ore was also used in a 100 kW CLC reactor where it was mixed with the oxygen carrier ilmenite. The manganese ore content was up to 8 wt% of the bed in these experiments and the solid fuel was two bituminous coals and wood char. It was seen that there was a significant decrease in the oxygen demand when manganese ore was mixed with the ilmenite[79].

1.4.5 Forms and availability of manganese ores

Manganese containing minerals have been found on all continents of the world, although most commercial deposits are from Africa[80]. Other large deposits can be found in Ukraine, Australia, India, China, Gabon and Brazil[80–83]. The elemental composition can vary extensively, as can be seen in Table 2. As manganese occurs naturally in three different oxidation states Mn^{+2}, Mn^{+3} and Mn^{+4}, manganese minerals may contain manganese in a multitude of different phases, e.g. braunite I/II (Mn_7SiO_{12}/$CaMn_{14}SiO_{24}$), bixbyite (Mn_2O_3), hausmannite (Mn_3O_4), jacobsite ($MnFe_2O_4$), manganite ($MnO(OH)$), tephroite (Mn_2SiO_4), pyrolusite (MnO_2), cryptomelane (KMn_8O_{16}), kutnahorite ($CaMn(CO_3)_2$), rhodochrosite ($MnCO_3$)[84–87] to mention a few.

1.5 Objective

The aim of this work is to evaluate manganese ores as a potential oxygen carrier for chemical looping combustion with gaseous and solid fuels. One important objective is to investigate the CLOU effect, or ability to release oxygen to the gas phase, as this could be highly beneficial for solid fuels. The objectives of determining the viability of manganese ores will be achieved using a combinations of experimental methods, including tests of a large number of materials in batch and continuously circulating reactors.

2 Experimental

2.1 Materials

A large number of ores from various suppliers around the world were obtained prior to and during the project. There are a large number of deposits and producers and it is sometimes difficult to obtain smaller sample quantities. In total, twenty different ores have, in some way, been tested in this work, see Table 2.

2.1.1 Preparation

Most of the manganese ores used in this work were prepared by heat treatment (calcination) in air at 950°C for 24 h using a box furnace, followed by crushing and sieving to obtain a particle size of 125-180 µm. In one study, several ores were evaluated without calcination, in which case they were simply crushed and sieved to obtain the same particle size of 125-180 µm. Additional preparation, such as epoxy casting and polishing, was done for ores analyzed with SEM-EDX (Scanning electron microscope – energy dispersive x-ray spectroscopy).

2.1.2 Characterization

2.1.2.1 Elemental analysis

The calcined ores were analyzed to determine their elemental composition through ICP-SFMS (Inductively Coupled Plasma – Sector Field Mass Spectrometry), see Table 2. The results are presented as the most thermodynamically favored metal oxide at the temperature of the heat treatment. It can be seen in the table that the ores generally have significant quantities of Fe and Si, and several ores also have high amounts of Ca and Mg (AN, AC). In addition to oxides, Table 2 lists the loss on ignition (LOI, i.e. weight reduction of the sample upon heating to 1000°C in air) that occurred during the elemental analysis of the ores. Here it was assumed that the metals are present as their most thermodynamically favored metal oxide at the heat treatment temperature. Thus, the composition is given as the most stable metal oxide at 950°C in air. As is evident, the amounts of metal oxides in the table do not always add up to 100%, but is somewhat lower for most ores, even when including the LOI, which was considerable for some of the ores. A high value of LOI could possibly be explained by the presence of carbonates and hydroxide species in the ore, or decomposition of pure or combined manganese oxides. Carbon dioxide was also detected during the initial heat up of some particles in the test reactor, which indicates that the calcination for 24 h at 950°C was not sufficient to calcine carbonates entirely. Further, the discrepancy in the analysis could be the result of the presence of oxides other than those used for the calculation in Table 2.

Table 2: Elemental analysis of most of the manganese ores investigated

Manganese Ore	Content [wt.%]											
	SiO_2	Al_2O_3	CaO	Fe_2O_3	K_2O	MgO	Mn_3O_4	Na_2O	P_2O_5	TiO_2	LOI*	Total
Buritirama (BR)	2.01	3.62	0.201	5.08	0.729	0.555	81	<0.05	0.133	0.182	1.4	95
Egyptian (EG)	1.89	0.6	2.03	14.6	0.146	1.63	70	0.509	0.14	0.0342	0.6	92
Gloria (GL)	6.07	0.22	12.4	8.37	<0.09	3.7	48	<0.05	0.048	0.0147	16	95
Metmin (MT)	12.6	3.14	0.831	51.4	0.408	0.189	22	<0.05	0.103	0.101	1.4	92
Nchwaning (NCH)	3.4	0.41	8.68	17.1	<0.09	1.01	59	0.0567	0.103	0.0494	6.4	96
Slovakian (SL)	6.5	0.36	11.6	5.9	0.401	2.98	51	0.195	0.052	0.0207	17	96
South African B (SAB)	4.6	0.35	8.34	17.3	<0.09	1.21	65	0.0537	0.084	0.0305	1.2	98
South African A (SAA)	3.7	0.5	5.54	23.3	<0.09	0.69	54	0.188	0.086	0.018	7.8	96
UMK (UMK)	2.0	3.9	0.24	5.45	0.709	0.56	86	<0.05	0.13	0.172	15	114
Tshipi (TS)	9.5	0.37	15.2	7.69	0.199	3.86	59	0.11	0.045	0.0254	0.9	97
Eramet HM (HM)	3.7	8.6	0.094	10.2	1.33	0.105	74	<0.05	0.3	0.228	0.9	99
Elwaleed Grade B (EB)	10	2.3	2.4	31	0.55	1.4	45	0.51	0.3	0.14	11	105
Elwaleed Grade C (EC)	9.8	2.4	1.2	74	0.32	0.65	16	0.41	0.22	0.12	0.5	106
Autlan Nodules (AN)	15	3.1	13	17	0.25	6.6	49	0.1	0.14	0.13	0.2	105
Autlan Carbonate (AC)	14	3.2	18	15	0.38	5.9	48	0.096	0.14	0.14	0.4	105
Sibelco Braunite (SB)	6.8	0.32	3.4	23	<0.09	0.62	76	<0.05	0.067	0.018	1	111
SinAus (SA)	8.4	4.7	1.3	13	1.3	0.36	73	0.28	0.22	0.2	0.7	103
Gui Zhou (GZ)	16	14	0.28	41	0.29	0.94	25	0.056	0.23	1.2	0.9	100
Sibelco Calcined (SC)	8	6.4	2.6	7.4	1.2	0.42	64	0.072	0.24	0.39	-1.6	89

**LOI= Loss on ignition, i.e. weight reduction of the sample upon heating to 1000°C in air*

2.1.2.2 Thermogravimetric analysis

The weight loss during heat-up of several ores were analyzed using a TA instrument Q-500 thermogravimetric analyzer (TGA), see Paper VI. Here, 15-20 mg of oxygen-carrier particles in the size range of 125-180 µm were heated from room temperature to 1000°C in air. The mass was continually measured during the cycling in order to gauge possible transformations in the ores during heat-up. Such transformations could be important with respect to use in pilot or commercial plants.

2.1.2.3 XRD and SEM-EDX

The manganese ores were also analyzed with x-ray powder diffraction (XRD) and, for some ores, SEM-EDX (Scanning electron microscope – energy dispersive x-ray spectroscopy). The analysis with XRD was done using a Siemens 5000 X-ray diffractometer with a copper source. The manganese ores were analyzed after heat treatment and sieving, using 125-180 µm particles. SEM-EDX analysis was done on heat treated particles cast in epoxy and then polished to expose the cross section inside the particles. An example showing the cross section of manganese ore particles are shown in Figure 7.

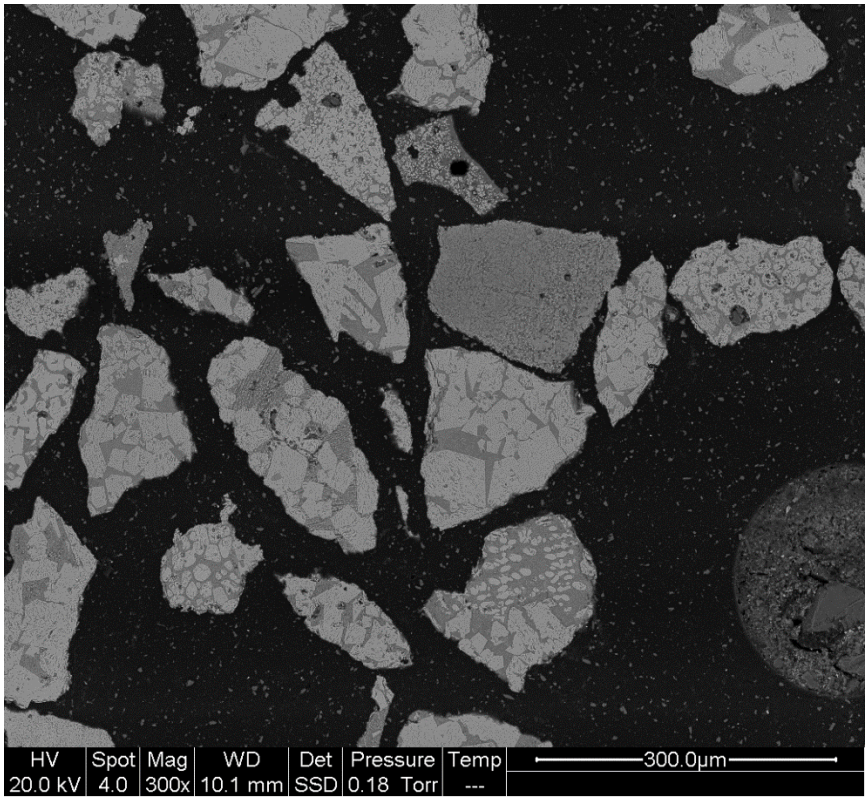

Figure 7: SEM image of cross section of manganese ore particles. This particular ore was calcined Gloria.

2.1.2.4 Crushing strength and BET

The crushing strength of the oxygen carrier particles was determined through the use of a Shimpo FNG-5 digital force gauge. Single particles were placed on the force gauge and then crushed, with the force required to break the particle registered. The process was repeated 30 times and then an average of the obtained results yields the crushing strength. A BET (Brunauer–Emmett–Teller**)** analysis were done on the ores to measure surface area. A Micromeritics Tristar 3000 was used with fresh and used particles, the latter ones tested in batch experiments.

2.1.2.5 Attrition

The ores were also investigated with respect to their mechanical strength and integrity in a jet-cup attrition rig at ambient conditions shown in Figure 8. To determine the rate of attrition, 5 g of particles are placed in the conical cup (13/25 mm conical inner diameter, 39 mm high) at the bottom of the apparatus. A nozzle with an inner diameter of 1.5 mm is located at the bottom of the cup, and tangentially in relation to the cup wall. During operation, air is added with a velocity of approximately 100 m/s through the inlet nozzle, creating a vortex of particles swirling upwards through the cup. Above the cup is a settling chamber, in which the gas velocity is reduced to below 0.005 m/s, allowing particles to fall back into the cup while fines (ideally <10 µm) are elutriated. The fines are collected in a filter at the top. The filter was removed and weighed every ten minutes. The total duration of an attrition test is one hour. A detailed description of the jet cup rig and methodology used for testing can be found elsewhere[88], including a comparison of attrition results and estimated lifetimes of a number of oxygen-carrier materials investigated in operation of CLC pilots. The high inlet gas velocity and the small inner diameter in the cup induce accelerated attrition, and for materials tested in actual operation, the attrition may be different. The particles evaluated in this rig were used, i.e. had been tested with methane and oxygen in the batch fluidized bed for several cycles at high temperature, see Table 4.

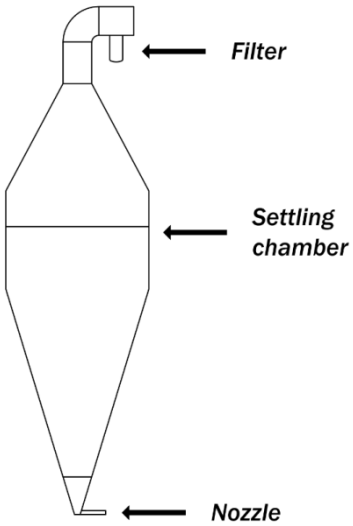

Figure 8: Schematic representation of the jet cup attrition rig[88].

2.2 Batch fluidized bed system

2.2.1 Setup of main reactor systems

The manganese ores were evaluated in a batch fluidized-bed reactor system consisting of an 820 mm long quartz reactor with an inner diameter of 22 mm. Particles are placed on a porous quartz plate placed 370 mm from the bottom. A CrAl/NiAl K-type thermocouple was used to measure the temperature 10 mm above the plate. The reactor is suspended in an electrical furnace and the pressure fluctuations is measured over the reactor to monitor fluidization. Gases are injected in the bottom of the reactor. As this is a batch reactor system, automatic valves are used to change the atmosphere inside the reactor in order to simulate alternately an air reactor and a fuel reactor. The gases are led from the reactor to a cooler, where water is condensed and removed. Thereafter the gases are led to a gas analyzer (Rosemount NGA 2000 multi-component gas analyzer), where volumetric flow and gas composition are measured. The analyzer measures, CH_4, CO, CO_2, and O_2. A schematic representation of the system used for the experiments can be seen in Figure 9.

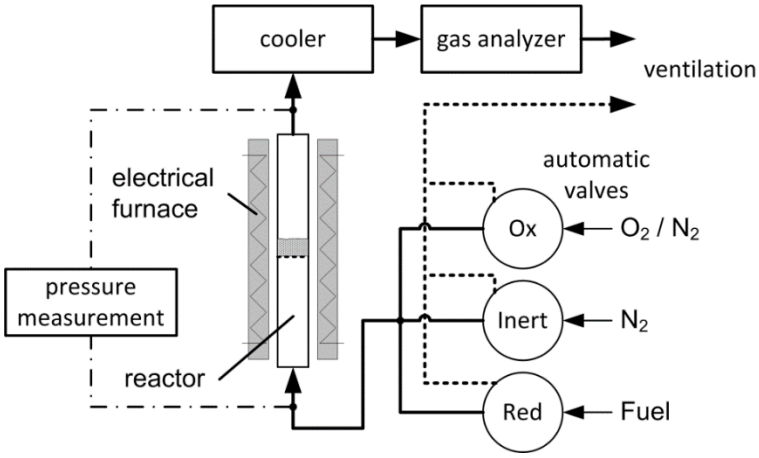

Figure 9: Schematic layout of the laboratory batch fluidized bed setup.

2.2.2 Procedure

The oxygen carrier particles are exposed to redox cycles in the batch fluidized-bed system. The first cycle is initiated after reaching the desired temperature, e.g. 850°C. One cycle consisted of: i) full oxidation of the sample at the initial temperature, in this case 850°C, using 5% O_2, ii) inert period of 60 s nitrogen to separate the oxidation and reduction period, iii) reduction of the sample with fuel for a period of, e.g., 80 s at 850°C, iv) inert period of 60 s nitrogen. After each cycle there is a reoxidation of the sample, which is also the first period of the subsequent cycle. This type of cycle is done with all of the fuels (solid fuel, methane, and syngas) although the reduction times will vary depending on the fuel used. After a series of cycles at the same temperature, the temperature may be changed, and this is done during an oxidation period.

2.2.2.1 Solid Fuel

The experiment was performed according to the experimental parameters listed in Table 3 with 15 g of oxygen-carrier particles in size range of 125-180 µm. In the solid fuel experiments, 0.1 g of

devolatilized wood char was inserted from the top of the reactor while the bed is fluidized with N_2. The primary purpose of these experiments was to evaluate the release rate of oxygen when the oxygen in the gas bulk is removed by char. By using an excess of char, the partial pressure of O_2 in the bulk is reduced to the very low level expected in a CLC fuel reactor. In this way, a rate of oxygen release can be calculated. It is important to stress that the aim of these experiments was not to gauge the char oxidation rate and reactivity, but rather the rate of oxygen transfer from the oxygen carrier particles.

Table 3: Experimental scheme for solid fuel experiments with devolatilized wood char as fuel. The abbreviations ox and red denote oxidation and reduction. Flows are normalized to 1 bar and 25°C.

No of Cycles	Reducing Agent	F_{ox} (mL_n/min)	F_{inert} (mL_n/min)	t_{inert} (s)	F_{red} (mL_n/min)	t_{red} (s)	T (°C)
3	Char	900	600	60	600	1500	850
3	Char	900	600	60	600	1500	900
3	Char	900	600	60	600	1500	950
3	Char	900	600	60	600	1500	1000

An example of a solid fuel cycle can be seen in Figure 10. The left figure shows the 2nd cycle with solid fuel at 950°C with the Gloria ore. The right figure shows the same typ of experiment but with sand as bed material. The vertical dashed line indicates when fuel was introduced to the particle bed. It is important to take note of the difference between the oxygen carrier case (a) and the sand case (b). In the left figure it can be seen that there is an initial large peak of CO_2, which then decreases with time. For the oxygen carrier case, the gas stream consists of CO_2, CO and N_2. In the sand case it can be seen that initially there are small peaks of CO and CO_2. The small peaks in the sand case could be due to a small amount of volatiles from the fuel despite previous devolatilization, or possibly from oxygen from the feeding of the solid fuel. However, it is clear that there is good conversion of solid fuel with the oxygen carrier, and very small or no converison with sand, as is expected. This illustrates that manganese ores can have an important CLOU effect.

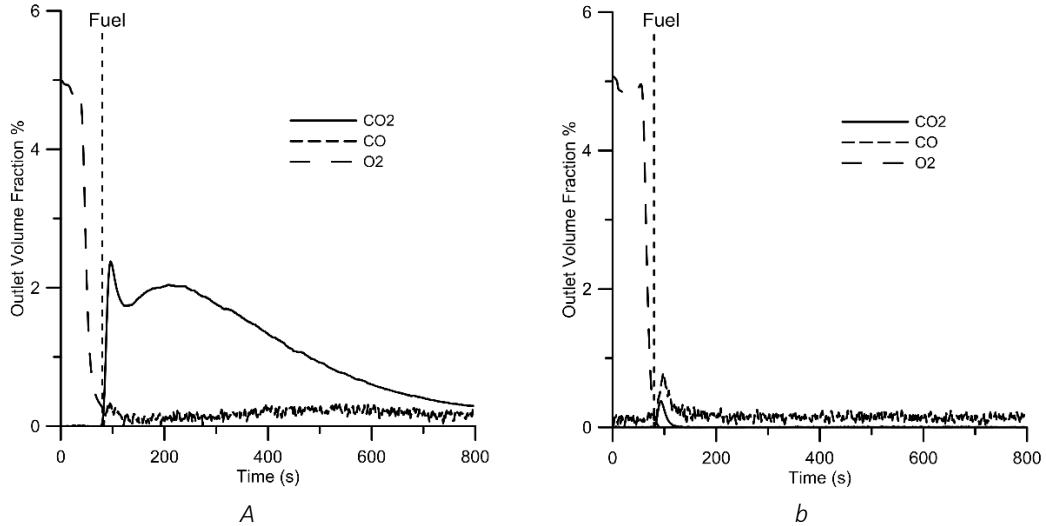

Figure 10: Gas concentrations from the second cycle with Gloria (a) and a cycle with sand (b) using char at 950°C.

2.2.2.2 Methane and oxygen release in nitrogen.

For the methane experiments, 15 g of oxygen carrier particles were used in the fluidized bed. Prior to the actual methane cycles, three syngas cycles were conducted to activate the material, see Table 4. After activation, three similar reduction cycles with methane were carried out for 20 s at 900°C, followed by three inert cycles, during which the reactor was fluidized with nitrogen for 360 s. The purpose of the inert cycles was to evaluate the oxygen release properties of the ores, i.e., the oxygen volume fraction from the outlet of the reactor. This was repeated at 950°C and 1000°C, after which the temperature was lowered to 900°C and two more reduction- respectively inert cycles were carried out. The last cycles at 900°C were performed to determine whether the oxygen carrier particles had maintained their original reactivity after experiencing redox cycles at higher temperatures.

Figure 11 shows an example of a methane cycle with Gloria manganese ore at 950°C. It starts with an oxidation period, after which nitrogen is introduced and the fraction of O_2 decreases gradually, as the particles are releasing some oxygen via the CLOU mechanism. The fuel is then introduced and oxidation reactions are initiated, which results in the formation of CO and CO_2. After the reduction period there is a 60 s inert period, which is followed by a new oxidation period. Initially all oxygen reacts with the oxygen carrier, but as the oxygen carrier approaches full oxidation, the oxygen concentration rises. In order to reach a stable level of O_2 additional 5 to 10 minutes are required (not shown here). Once this level is reached, the particles are considered to be fully oxidized.

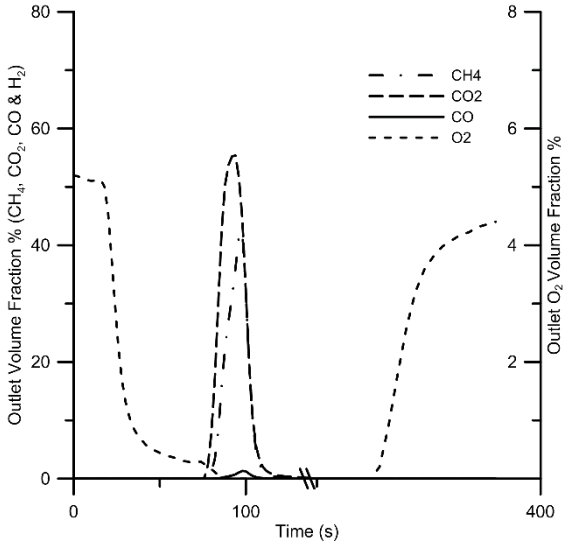

Figure 11: The gas concentrations from the second methane cycle (using15 g oxygen carrier) for the Gloria manganese ore at 950°C.

Four uncalcined (untreated) ores were also evaluated with methane using the batch fluidized bed reactor in order to compare the reactivity to the heat treated materials. The procedure was similar to that outlined in Table 4, but only a temperature of 950°C was used, as this temperature is commonly employed in CLC pilots. There were four ores selected for these experiments, Tshipi (TS), Nchwaning (NCH), Sibelco Braunite (SB) and Buritirama (BR).

Table 4: Experimental scheme of gaseous fuel experiments with methane and 15 g bed of particles. The abbreviations ox and red denote oxidation and reduction, respectively. Flows are normalized to 1 bar and 25°C.

No of Cycles	Reducing gas	F_{ox} (mL_n/min)	F_{inert} (mL_n/min)	t_{inert} (s)	F_{red} (mL_n/min)	t_{red} (s)	T (°C)
3	Syngas	900	600	60	450	80	850
3	Methane	900	600	60	450	20	900
3	Nitrogen	900	600	360	-	-	900
3	Methane	900	600	60	450	20	950
3	Nitrogen	900	600	360	-	-	950
3	Methane	900	600	60	450	20	1000
3	Nitrogen	900	600	360	-	-	1000
2	Methane	900	600	60	450	20	900
2	Nitrogen	900	600	360	-	-	900

2.2.2.3 Syngas

In contrast to the experiments with methane, syngas experiments were performed with 2 g of oxygen carrier mixed with 13 g of sea sand, both with a size range of 125 to 180 µm. The low bed mass is due to a much higher reactivity of the oxygen carriers towards syngas as compared to methane. This means that if larger amounts of oxygen carriers were used, full conversion of gas would be approached, which would make comparison difficult. Otherwise, setup and flows were similar. The experimental parameters for the syngas experiments are listed in Table 5. The reduction time was 20 s and the inert periods were 60 s. Three cycles were performed at each temperature. After three cycles at 1000°C, the temperature was decreased to 950°C and 13 additional cycles were conducted. This was done in order to assess whether conversion was affected by the number of cycles.

Table 5: Experimental scheme for gaseous fuel experiments with syngas. The abbreviations ox and red denote oxidation and reduction. Flows are normalized to 1 bar and 25°C.

No of Cycles	Reducing gas	F_{ox} (mL_n/min)	F_{inert} (mL_n/min)	t_{inert} (s)	F_{red} (mL_n/min)	t_{red} (s)	T (°C)
3	Syngas	900	600	60	450	20	850
3	Syngas	900	600	60	450	20	900
3	Syngas	900	600	60	450	20	950
3	Syngas	900	600	60	450	20	1000
13	Syngas	900	600	60	450	20	950

2.2.3 Data evaluation

Fuel conversion, or the CO_2 yield, γ, from syngas (CO) and methane conversion is defined as in (Eq. 1) and (Eq. 2) respectively. The oxygen carrier mass-based conversion, ω, represents the degree of oxidation of the oxygen carrier, (Eq. 3), where ω = 1 corresponds to fully oxidized material. In (Eq. 3), m is the actual mass of the oxygen carrier and m_{OX} is the mass of the fully oxidized oxygen carrier. p_x is the partial pressure of gas species x.

$$\gamma_{CO} = \frac{P_{CO_2}}{P_{CO_2} + P_{CO}} \quad \textit{(Eq. 1)}$$

$$\gamma_{CH_4} = \frac{P_{CO_2}}{P_{CO_2} + P_{CO} + P_{CH_4}} \quad \textit{(Eq. 2)}$$

$$\omega = \frac{m}{m_{OX}} \quad \textit{(Eq. 3)}$$

From a mass balance over the reactor, ω, can be calculated for each time step, for CH_4 (Eq. 4), syngas (Eq. 5) and for char (Eq. 6). The partial pressure of hydrogen is not measured but assumed to react at the same rate as CO, which is a conservative assumption. In a few papers, hydrogen was calculated assuming equilibrium of the water gas shift reaction.

Methane: $\omega_1 = \omega_0 - \int_{t_0}^{t_1} \frac{\dot{n}_{out} M_o}{m_{ox} P_{tot}} \left(4P_{CO_2,out} + 3P_{CO,out} - P_{H_2,out}\right) dt$ *(Eq. 4)*

Syngas: $\omega_1 = \omega_0 - \int_{t_0}^{t_1} \frac{\dot{n}_{out} M_o}{m_{ox} P_{tot}} \left(2P_{CO_2,out} + P_{CO,out} - P_{H_2,out}\right) dt$ *(Eq. 5)*

Char: $\omega_1 = \omega_0 - \int_{t_0}^{t_1} \frac{\dot{n}_{out} M_o}{m_{ox} P_{tot}} \left(2P_{CO_2,out} + P_{CO,out}\right) dt$ *(Eq. 6)*

The attrition index is calculated from attrition tests in the jet cup setup according to (Eq. 7), where the difference in the numerator is the weight fraction lost in the last 30 minutes of a 60 minute test. Multiplication by two, i.e. 60/30, yields the corresponding weight loss in % per h.

$$AI = \frac{wt\%_{t_{60}} - wt\%_{t_{30}}}{30} * 60 \quad \textit{(Eq. 7)}$$

2.3 Circulating fluidized bed system

2.3.1 Setup

The circulating fluidized bed system is a 300W laboratory-scale chemical-looping reactor, see Figure 12. The purpose of the reactor is to evaluate oxygen carriers with continuous circulation and continuous fuel feed. The reactor is 300 mm high and the fuel reactor has a cross section of 25x25 mm. The air reactor has a base of 25x42 mm and contracts to 25x25 mm in the riser section. Fuel and air enter the system through separate windboxes, located at the bottom of each reactor. The gas distributors are porous quartz plate. See paper V for more details.

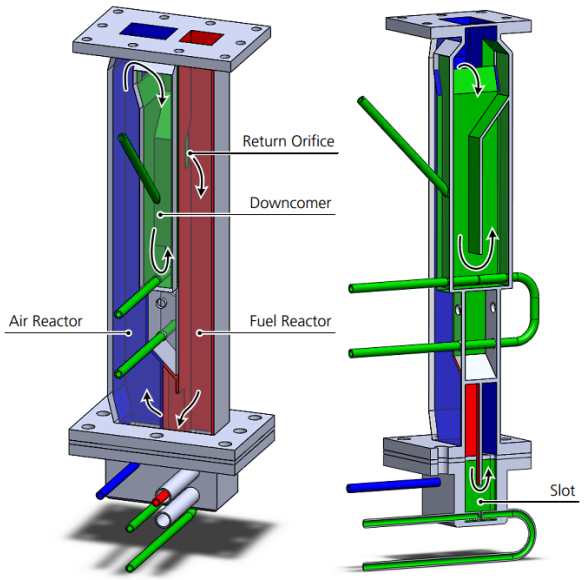

Figure 12: Illustration of the 300W circulating fluidized-bed unit. (Taken from Paper V)

2.3.2 Procedure

The ores used in the circulating system were selected based on the elemental composition of the ores, see Table 2. All materials were heat treated for 24 h at 950°C prior to operation in the circulating system. The idea behind the selection for this particular study was to evaluate ores with varying composition with respect to Ca/Mn, Fe/Mn and Si/Mn. As is evident from Table 2, Elwaleed C is Fe-rich, Gui Zhou is also Fe-rich, but with high amounts of Si. Both Tshipi and Sibelco Braunite are Mn-rich, but Tshipi also has considerable amounts of Ca. During the experiment in the 300W unit the bed volume was kept roughly constant, which corresponds to 310-400 g of oxygen carrier. The ores were investigated with biomass volatiles, methane and syngas between 800-950°C. In the thesis, only results of the syngas and methane experiments will be discussed, and the reader is referred to Paper V for more details regarding the biomass volatile experiments. The experimental procedure can be seen in Table 6. Attrition of the oxygen carrier materials was determined through measurement of the amount of fines (particles smaller than 45 µm) produced during operation.

Table 6: Experimental parameters for the circulating fluidized bed system

	Elwaleed C (EC)	Tshipi (TS)	Gui Zhou (GZ)	Sibelco Braunite (SB)	Morro da Mina (MM)
Solid inventory (g)	380	310	330	400	280
Particle size (µm)	90-212	90-212	45-212	45-250	90-212
CH_4 (kg/MWth)	397	-	225-337	437	-
Syngas (kg/MWth)	250-380	260	220-300	330-430	-
Operation time CH_4 (h)	3.9	-	14.6	3.1	-
Operation time Syngas (h)	8.7	3.1	6.0	9.8	-

2.3.3 Data Evalution

The evaluation of the conversion of carbon uses data from different analyzers, i.e., infrared analyzers (IR) and a gas chromatograph (GC). Carbon fractions, $f_{C,i}$, are calculated, which are the fractions of fuel carbon in the fuel reactor converted to CO, CO_2, CH_4 and higher hydrocarbons than CH_4 (C2 and C3), see (Eq. 8)–(Eq. 12). The term "yield" instead of fraction is used for the carbon fraction of CO_2, see (Eq. 8).

$$\gamma_{CO_2}=\frac{x_{CO_2,FR}}{x_{CO_2,FR}+x_{CO,FR}+\sum(m*x_{C_mH_n,FR})} \quad \textit{(Eq. 8)}$$

$$f_{CO}=\frac{x_{CO,FR}}{x_{CO_2,FR}+x_{CO,FR}+\sum(m*x_{C_mH_n,FR})} \quad \textit{(Eq. 9)}$$

$$f_{CH_4}=\frac{x_{CH_4,FR}}{x_{CO_2,FR}+x_{CO,FR}+\sum(m*x_{C_mH_n,FR})} \quad \textit{(Eq. 10)}$$

$$f_{C_2}=\frac{\sum(2*x_{C_2H_n,FR})}{x_{CO_2,FR}+x_{CO,FR}+\sum(m*x_{C_mH_n,FR})} \quad \textit{(Eq. 11)}$$

$$f_{C_3}=\frac{\sum(3*x_{C_3H_n,FR})}{x_{CO_2,FR}+x_{CO,FR}+\sum(m*x_{C_mH_n,FR})} \quad \textit{(Eq. 12)}$$

3 Results

3.1 Reactivity in the batch fluidized bed system

3.1.1 Oxygen release to the gas phase

The ability of the manganese ores to release oxygen to the gas phase, i.e. oxygen uncoupling property, was investigated in the batch fluidized-bed system. This was done by measuring the O_2 concentration in the inert period following an oxidation period, see Section 2.2.2.2. Several redox cycles were done prior to the inert period. This was done to achieve a certain level of phase stabilization within the material, i.e. to minimize the risk that any unstable oxides present in the original samples, e.g. MnO_2 or pure Mn_2O_3, would not contribute to the oxygen release, see Figure 3. These phases are not expected to be formed in the air reactor.

Figure 13 shows the outlet oxygen volume fraction for three manganese ores at 950°C during the inert period. Here, the oxygen back mixing has been accounted for, by taking the difference between outlet O_2 of the oxygen carrier experiment with a similar experiment conducted with sand as bed material. It can be seen that there is an initial peak of oxygen released after the inert gas is introduced to the sample. As the oxygen available for release through CLOU diminishes the oxygen in the outlet gas decreases.

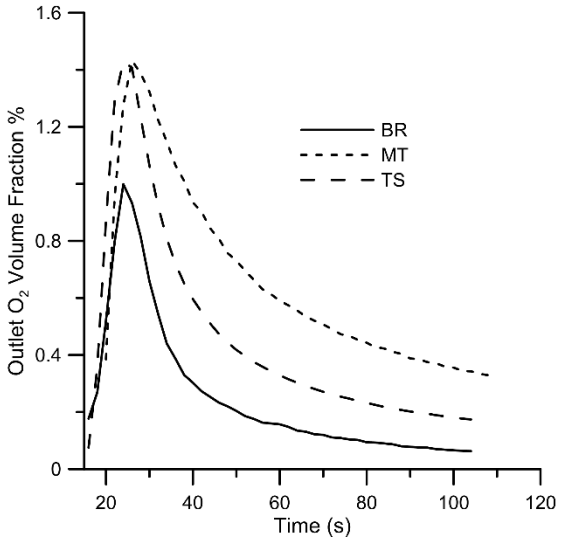

Figure 13: Outlet O_2 volume fraction as a function of time for three ores at 950°C during the inert period when the particles were fluidized with only N_2.

.

Figure 14a and Figure 14b show the average concentration of O_2 in the outlet gas from the reactor at 900°C, 950°C and 1000°C when oxygen is released into a flow of N_2. The concentrations shown are averages based on a 90 s period from 15 s to 105 s in the inert period. Thus the maximum concentrations could actually be somewhat higher. It can be seen that the ores generally release more oxygen as the temperature is increased, although the temperature dependence differs. The fact that there is some oxygen release from all ores and at all temperatures suggests the presence of combined oxides, as thermodynamically Mn_2O_3 cannot be oxidized with 5% O_2 above 800°C, see Figure 3. The extent of the oxygen release varies greatly among the ores. The four ores with highest oxygen release are Metmin (MT), Gui Zhou (GZ), Elwaleed Grade C (EC), and Sibelco Braunite (SB). Interestingly, the first three ores are iron-rich minerals, see Table 2. This may

explains the higher degree of oxygen release for these particles, as a higher fraction of Fe in the Fe/Mn-system promotes the oxygen release reactions at higher temperatures[51], see Figure 4. A clear two-phase region of bixbyite and spinel is present in the Fe/Mn-system at relevant temperatures, which is not the case for low contents of Fe compositions meaning that oxidation to bixbyite is not possible at these conditions.

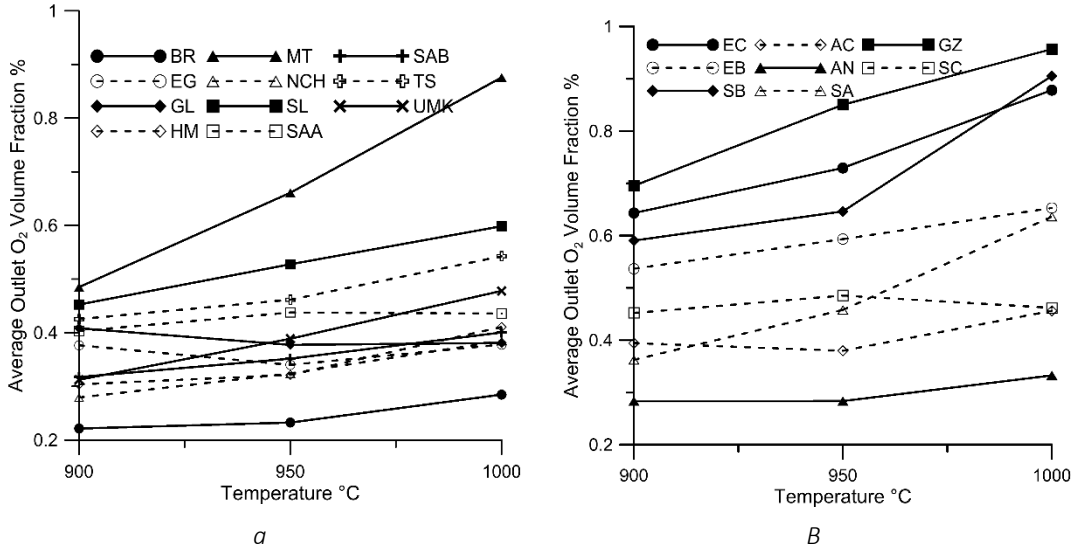

Figure 14: Average volume fractions of O_2 in the outlet gas stream over a period of 90 s at temperatures 900°C, 950°C and 1000°C. The ores from Paper II shown in a and from Paper III in b.

It should also be noted that although the amount of oxygen released from these ores during the inert period corresponds to a conversion of 0.01-0.03 mass% of the oxygen carrier, the release rate will be considerably higher when the driving force is increased, i.e. if oxygen is removed from the gas phase by the fuel. This was shown by Arjmand et al.[70], where the Brazilian manganese ore (BR) released 0.25-0.3 mass% of O_2 over the course of 15 min when 0.1 g of low-volatile fuel was added in an N_2 atmosphere. Similar types of experiments were thus performed with several ores in this work, see Paper IV.

Six ores were selected to be investigated with respect to their oxygen release rates using wood char to remove the oxygen in the bulk via combustion. During these experiments, 0.1 g of wood char was inserted per cycle. The excess char ensures that the bulk oxygen concentration is low, similar to conditions expected in the fuel reactor. Figure 15 shows a comparison between oxygen removed by an inert N_2 flow and oxygen removed by wood char for Gloria manganese ore at different temperatures. It can be seen that the oxygen carrier particles are only slightly reduced during the inert cycles, in stark contrast to the reduction cycles with char present in the bed. In fact, almost 1 mass% is removed as oxygen at 1000°C. In the nitrogen case the conversion achieved was only 0.048 mass% at 1000°C (however calculated for a different time span than Paper II), see Paper IV. These two cycles with inert conditions can be seen in the top part of the figure, however, they overlap due to the small difference in oxygen release. Clearly, the use of char in the bed results in an enhanced driving force for oxygen release, and may be a more appropriate way of gauging the CLOU effect.

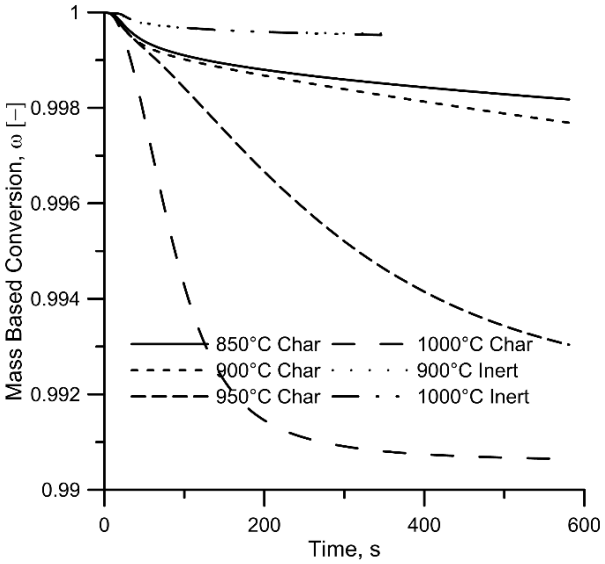

Figure 15: Mass-based oxygen carrier conversion as a function of time for 15 g of Gloria manganese ore with 0.1 g of devolatilized wood or char. The figure shows reduction cycles with char between 850°C and 1000°C and reduction cycles with inert atmosphere at 900°C and 1000°C (overlap).

Figure 16 shows a comparison of the conversion rates of oxygen carriers investigated with wood char at temperatures ranging from 850°C to 1000°C. The rates are determined during a 20 s period from t=40 s to t=60 s. Gloria and Tshipi had the highest conversion rates with solid fuel, which was rather unexpected, based on the intermediate oxygen release in nitrogen shown in Figure 14. They both convert solid fuel faster than Gui Zhou and Metmin, the two ores which showed the highest rate and oxygen capacity using inert gas only. This may mean that the mechanism for oxygen transfer changes as the partial pressure of oxygen is decreased. In the figure, only three points can be seen for SinAus, which can be explained by agglomeration in the last cycle at 950°C.

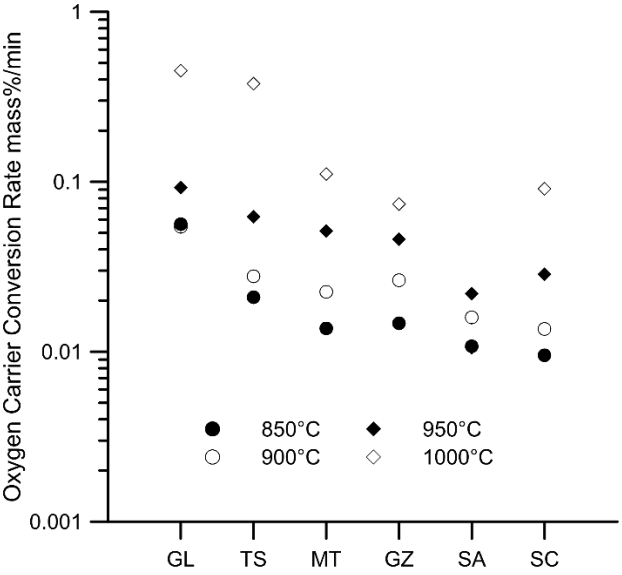

Figure 16: Oxygen carrier conversion rates at temperatures ranging from 850°C to 1000°C with 15 g of oxygen carrier with 0.1 g of devolatilized wood char. The rates were taken from the 20 s period between t=40 s to t=60 s of the reduction period.. GL=Gloria, TS=Tshipi, MT= Metmin, GZ= Gui Zhou, SA= SinAus, and SC= Sibelco Calcined.

3.1.2 Methane Reactivity

In the investigations with methane, 15 g of oxygen carrier particles were used, and these were fluidized using CH_4. Figure 17a (left) shows the CO_2 yield from methane, γ_{CH_4}, as a function of the degree of mass-based conversion, ω, for the ore South African A (SAA) at three different temperatures. It can be seen that as the temperature is raised, the CO_2 yield increases. This trend was general for all ores investigated. Figure 17b shows the CO_2 yield as a function of degree of mass-based conversion, ω, for the nine manganese ores investigated in Paper III. It can be seen that there is a large difference in CO_2 yield between the ores spanning from 5% (AN) to 80% (EB) at 950°C initially. The gas yield decreases as a function of time for all oxygen carriers. For instance, at a conversion level of ω=0.995, the gas yield, and hence reactivity, of EB ore decreases to 40%. In other words, when the conversion of the oxygen carrier is reduced by 0.5 mass% its reactivity towards methane is half of what it was initially.

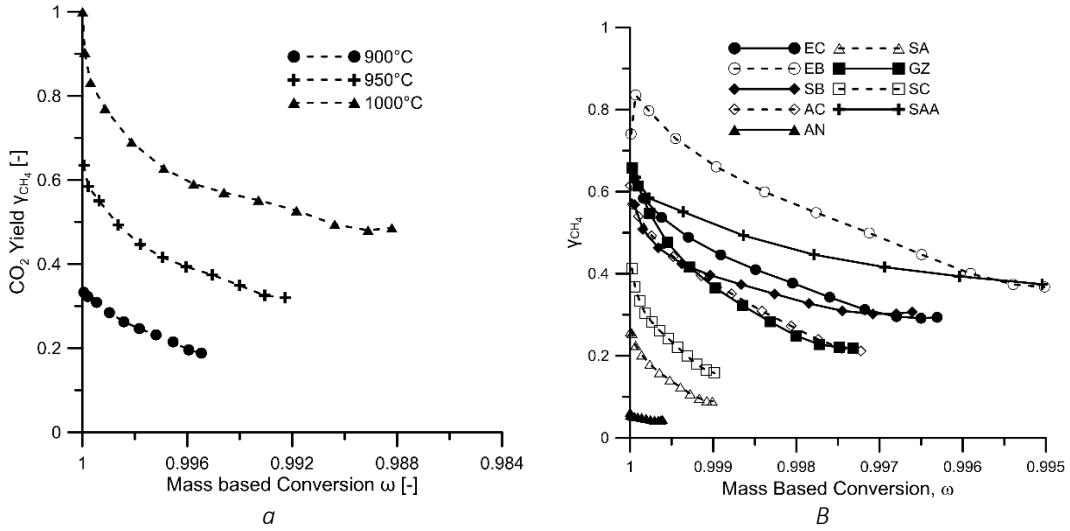

Figure 17: CO_2 yield of methane (γ_{CH_4}) as a function of the mass-based conversion (ω) for SAA ore at 900°C, 950°C and 1000°C is shown in Figure 17a. Figure 17b shows the CO_2 yield (γ_{CH_4}) as a function of ω for several ores during the second methane cycle at 950°C.

Figure 18a and Figure 18b show the average CO_2 yield from the methane experiments for all ores investigated. The average CO_2 yield from methane, γ_{CH_4}, is based on the whole reduction period and varies significantly among the different manganese ores. The Gloria ore exhibited the best gas conversion with an average CO_2 yield of slightly below 80% at 1000°C. Still, the reactivity varies in a wide range. The highest CO_2 yields are seen for the ores that achieved high levels of oxygen release in the solid fuel experiments, i.e. GL and TS. The reactivity for the iron –rich ores Gui Zhou, Metmin, and Elwaleed grade C, usually achieve low to intermediate values of gas yield.

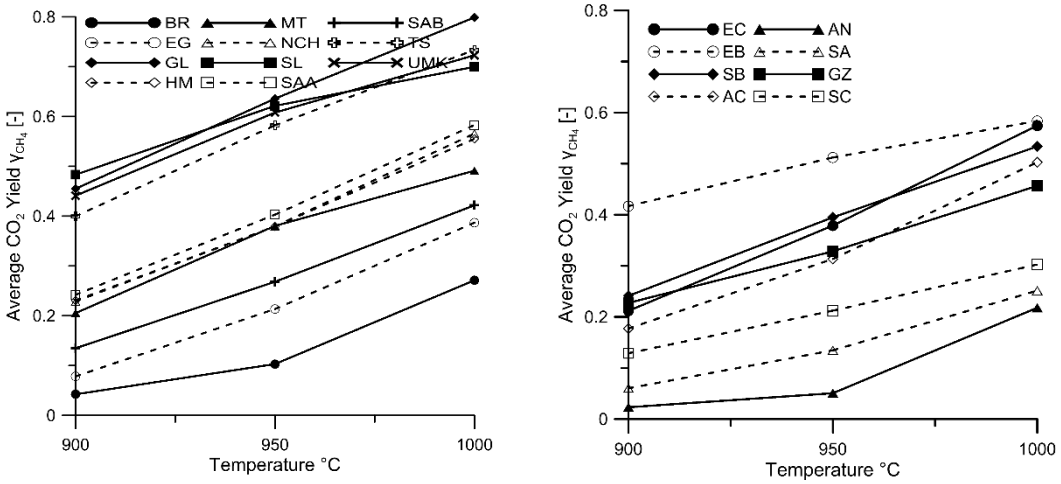

a *b*

Figure 18: The average CO_2 yield of methane (γ_{CH_4}) is shown in Figure 18a and Figure 18b for all the manganese ores (11+8) at 900°C, 950°C and 1000°C.

Two sequences of reducing periods at 900°C were conducted with methane – one before and one after the cycles at 950°C and 1000°C, see Table 4. As explained earlier, the idea here was to gauge the possible influence on reactivity of the high temperature cycles. Figure 19 shows the average CO_2 yield for these two sequences at 900°C for the ores from Figure 18a, investigated as a part of Paper II. It can be seen that most ores showed a decrease in reactivity after the cycles at 1000°C, which is also true for the ores represented in Figure 18b, see Paper III. There are exceptions such as the South African A ore (SAA), whose average CO_2 yield increased by about 40%. The decrease that most other ores exhibited is likely to have implications with respect to methane combustion, as the solid inventory is related to the reactivity. The effect seen is not necessarily solely a result of the high temperature, but the decreasing reactivity could be a gradually process occurring even at lower temperatures, albeit at a slower rate. This decreasing reactivity as a function of cycle has been seen for some ores, while others have been rather stable, e.g. Figure 28.

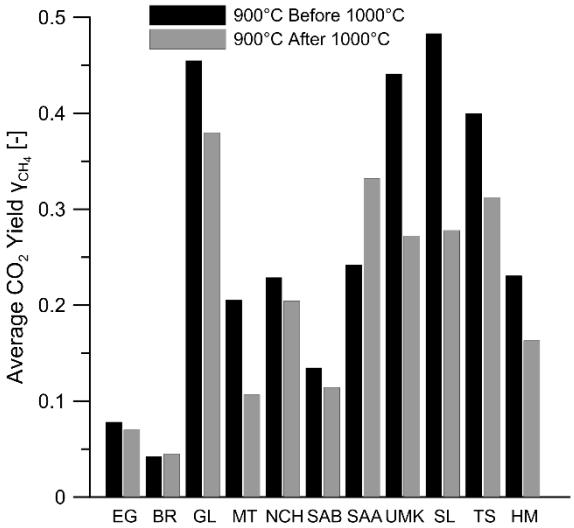

Figure 19: Average CO_2 yield (γ_{CH4}) from methane at 900°C before and after the cycles at 950 and 1000°C.

3.1.3 Syngas Reactivity

The reactivity of syngas (50/50 vol%, H_2/CO) is particularly interesting for combustion of solid fuels, where CO and H_2 are important intermediates, see Section 1.4. Experiments were carried out in a similar manner as with methane, the main exception was that only 2 g of oxygen carrier was used, see Section 2.2.2.3. Figure 20 shows the results of syngas experiment for eight investigated managanese ores (Paper III). All ores show decreasing reactivity as a function of mass based conversion, and there is a large variation in the CO_2 yield between the different ores.

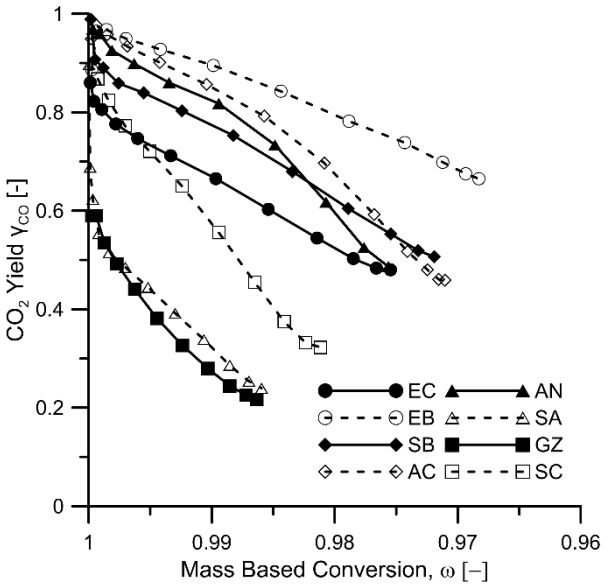

Figure 20: CO_2 yield (γ) as a function of mass-based conversion of the oxygen carrier (ω) for the second syngas cycle at 950°C.

Figure 21a and Figure 21b show the average CO_2 yields for the 19 ores tested with syngas at temperatures from 850°C to 1000°C. The average gas yield is calculated over the entire reduction period. It can be seen that there is a large difference in reactivity among the ores as the average CO_2 yields vary between 20% and 90% at these temperatures. The manganese rich ores, molar Fe/Mn<1, in general had varying reactivity. The iron rich ores, molar Fe/Mn>1, generally had low reactivity, with a CO_2 yield lower than 60% at 950°C. Interestingly, several of the ores which had the highest average methane conversion (>50% at 950°C) were also among the ores with the highest CO conversion (>80% at 950°C), i.e. TS, GL, SL and UMK. The first three of these are characterized by a high Ca/Mn and Mg/Mn ratio, as seen in Table 2.

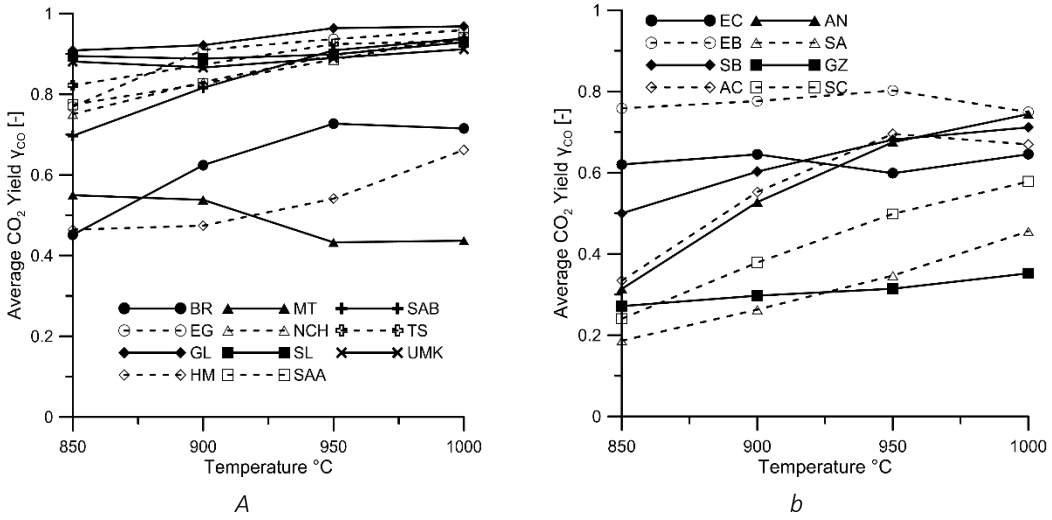

Figure 21: The average CO_2 yield for CO is shown in Figure 21a and Figure 21b for all manganese ores with 2 g at different temperatures.

Similar to the methane test series, the reactivity towards CO decreased for most ores over the cycles at 1000°C, see Paper II and III. In order to investigate the stability of the particles beyond that point additional 13 redox cycles were performed with syngas. These cycles were conducted at 950°C, see Figure 22a and Figure 22b. It can be seen that the reactivity of the ores is relatively stable but for some ores there is a slight decrease in reactivity. In some cases such as for Gui Zhou (GZ) and SinAus (SA) there was a slow increase in CO_2 yield over the course of the 13 cycles.

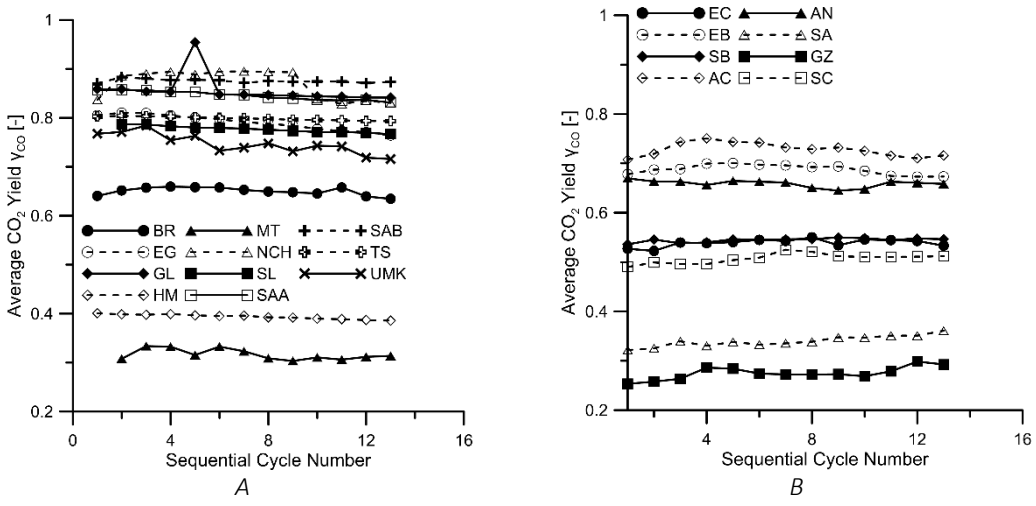

Figure 22: Average CO_2 yield for 13 consecutive cycles with syngas at 950°C following the cycles at 1000°C. See Table 5 for more details.

3.1.4 Relative reactivity performance

From the results presented with respect to the reactivity with methane, CO and char it is apparent that the reactivity varies in a wide range and is very dependent upon the ore investigated as well as the fuel. The reasons for the differences could have many explanations, and the variation in elemental compositions, see Table 2, opens up for the possibility of different phase transitions

during the redox cycling. This could explain the wide range of results seen even with the same fuel. Figure 23 shows the correlation between methane and CO reactivity. Although there is a trend of increasing CO yield with CH_4 yield, there is a large spread in the data.

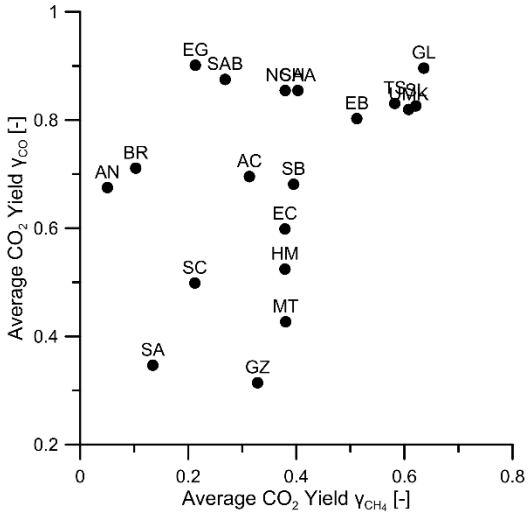

Figure 23: Comparison between the average CO_2 from methane and CO at 950°C

Further, Table 7 presents a relative ranking of the ores based on reactivity with methane, CO and oxygen release (inert and with char) at 950°C. The results are ordered according to performance with respect to reactivity and oxygen release. There are several ores which have a high reactivity with both fuels and also a high rate of oxygen uncoupling, most notably TS and GL.

In Paper II it was seen that the gas yield of CO was correlated to the alkali content, more specifically potassium. Figure 24a and b shows the average CO_2 yield for CO and CH_4 as a function of the molar ratio of K/(K+Mn) for all of the investigated materials. This shows that there is a general trend of decreasing reactivity with increasing K, however again there is a large spread in the data.

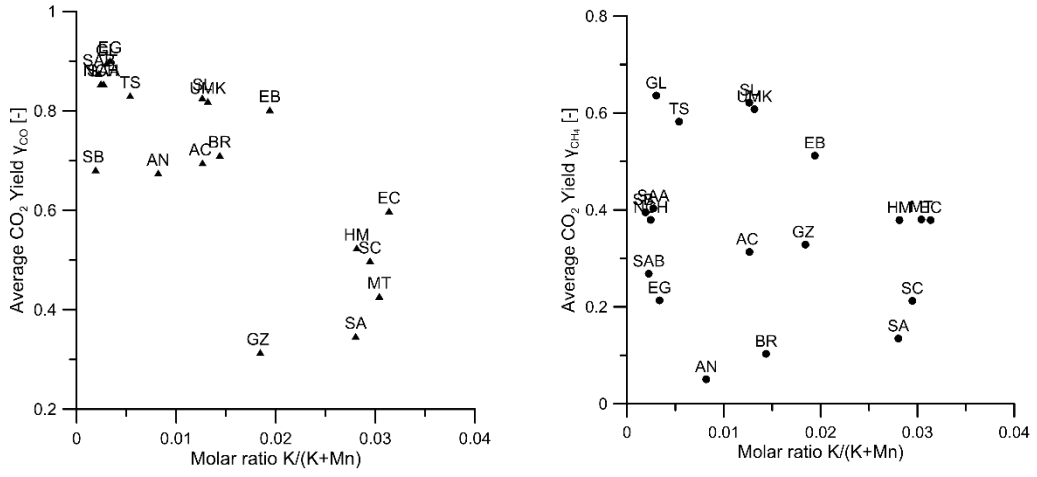

a *b*

Figure 24: Average CO_2 yield for CO and CH_4 as a function of molar ration of K/(K+Mn) shown in a and b respectively

Table 7: Summarized results from syngas, methane, and oxygen release experiments at 950°C. Ordered according to reactivity performance.[*]

Performance Rank	Uncoupling O_2	Uncoupling char	CH_4	Syngas
1	GZ (0.85)	GL (0.09)	GL (0.64)	EG (0.9)
2	EC (0.73)	TS (0.06)	SL (0.62)	GL (0.9)
3	MT (0.66)	MT (0.05)	UMK (0.61)	SAB (0.88)
4	SB (0.65)	GZ (0.05)	TS (0.58)	NCH (0.85)
5	EB (0.59)	SC (0.03)	EB (0.51)	SAA (0.85)
6	SL (0.53)	SA (0.02)	SAA (0.4)	TS (0.83)
7	SC (0.49)	-	SB (0.39)	SL (0.83)
8	SA (0.46)	-	MT (0.38)	UMK (0.82)
9	TS (0.46)	-	NCH (0.38)	EB (0.8)
10	SAA (0.44)	-	HM (0.38)	BR (0.71)
11	UMK (0.39)	-	EC (0.38)	AC (0.7)
12	GL (0.38)	-	GZ (0.33)	SB (0.68)
13	AC (0.38)	-	AC (0.31)	AN (0.67)
14	SAB (0.35)	-	SAB (0.27)	EC (0.6)
15	EG (0.34)	-	EG (0.21)	HM (0.52)
16	NCH (0.32)	-	SC (0.21)	SC (0.5)
17	HM (0.32)	-	SA (0.13)	MT (0.43)
18	AN (0.28)	-	BR (0.1)	SA (0.35)
19	BR (0.23)	-	AN (0.05)	GZ (0.31)

[*] Values in parentheses: O_2(Average O_2 outlet volume fraction), Char (mass%/min), CH_4 (average γ_{CH_4}), Syngas (average γ_{CO})

Two additional important components which are quite variable with respect to the elemental composition, see Table 2, are Fe and Ca. The average gas yield for CO is shown as a function of Fe/(Fe+Mn) and Ca/(Ca+Mn) in Figure 25a and b respectively. Although big variations there is a general trend of increasing reactivity with increasing Ca and decreasing Fe. Notably TS, GL and SL have among the highest fraction of Ca of all ores, and they are among the most reactive ores for all fuels. Further, they also have significant rates of oxygen uncoupling, as seen in Table 7. Additional elements of high interest for CLOU are Si and Mg. For the former, no significant trend could be observed, although manganese silicates could still be an active component in the oxygen transfer process, see Paper III. With respect to magnesium the trends in reactivity followed that of Ca to a large extent. It should be stressed that the chemistry of these ores is very complex, and that no statistical significant conclusions can likely be drawn with respect to correlations of reactivity with composition.

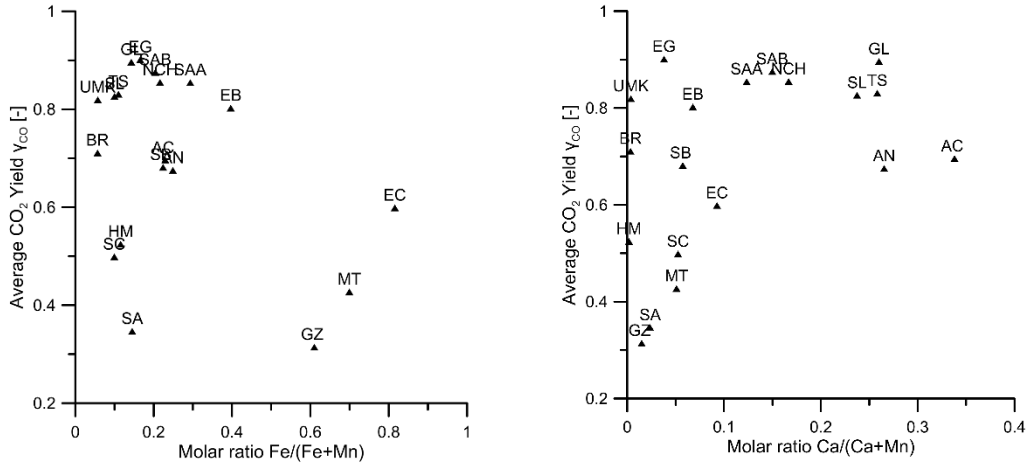

Figure 25: Average CO_2 yield for CO as a function of molar ration of Fe/(Fe+Mn) and Ca/(Ca+Mn) shown in a and b respectively.

3.1.5 Apparent Kinetics

From the results presented in Section 3.1.2 and Section 3.1.3 with CH_4 and CO it is clear that the reactivity of the heterogeneous ores vary extensively, but there is a general decrease in reactivity as a function of mass based conversion (ω), see Figure 17b and Figure 20. No attempt was made to model the gas-solid reaction using functional relationships of mass based conversion (ω) vs temperature (T). However, effective rate constants were calculated for the two fuels, see (Eq. 13) for CO and (Eq. 14) for CH_4. Further, it was assumed that the temperature dependence on the reactivity follows an Arrhenius type expression, i.e. (Eq. 15), where A is the frequency factor and E_a the activation energy. Figure 26 shows the Arrhenius plots based on the reaction constants presented in Paper III.

$$k_F(\omega) = \frac{-\ln(1-\gamma_{CO})n_{in}}{m} \quad \text{(Eq. 13)}$$

$$k_F(\omega) = \frac{n_{in}((1+\varepsilon)\ln\left(\frac{1}{1-\gamma_{CH_4}}\right) - \varepsilon\gamma_{CH_4}}{p_{CH_4,in}m} \quad \text{(Eq. 14)}$$

$$k_F = Ae^{-\frac{E_a}{RT}} \quad \textit{(Eq. 15)}$$

For more details and definitions, see Paper III and IV. The rate constant k_F has earlier been used to model gas conversion in several pilot units[89,90]. The main assumptions in this work when deriving k_F for CH_4 and CO were:

- The reactions is of the first-order with respect to the reactive fuel component
- The reactor is a plug flow reactor with respect to the gas phase.
- Reactions are taking place in the temperature range of 900-1000°C.
- All oxygen carriers are at the same degree of conversion.
- The impact of the oxygen released through the CLOU mechanism on the rate constant is not significant.
- The amount of CO converted through the water-gas shift reaction is negligible.

Figure 26a (left) shows Arrhenius plots for the CH_4 cases. Here, the reaction constants were calculated at a solids conversion of ω=0.999. However, for SA and AN, data was taken at ω=0.9995 and ω=0.9998, respectively, since an oxygen carrier conversion of ω=0.999 could not be reached. Figure 26b (right) shows Arrhenius plots for the CO cases, where the reaction constant for the ores were calculated at a solids conversion of ω=0.99. From Figure 26b it can be seen that two ores show low dependency on temperature. One of these are EC which defluidized during the experiment, which may explain the low temperature dependence. The other oxygen carrier, EB shows only a slight change in the rate constant as a function of temperature.

For the CO case there results are more varied than in the methane case, this could be because of the smaller amount of oxygen carrier material in the bed which would make it more sensitive to changes. The activation energies for the ores vary considerably, in the range 10-168 kJ/mole for CO and 110-328 kJ/mole for methane. The explanation for this large span could be due to many reasons including different mechanisms of mass transport and also different active components transferring oxygen.

The activation energy for the CLOU reaction was also determined for several ores, see Paper IV. Here it was also established that although the uncoupling capacity was significant for a few ores, the rates of oxygen transfer were generally much lower than the rates of transfer to the gaseous fuel.

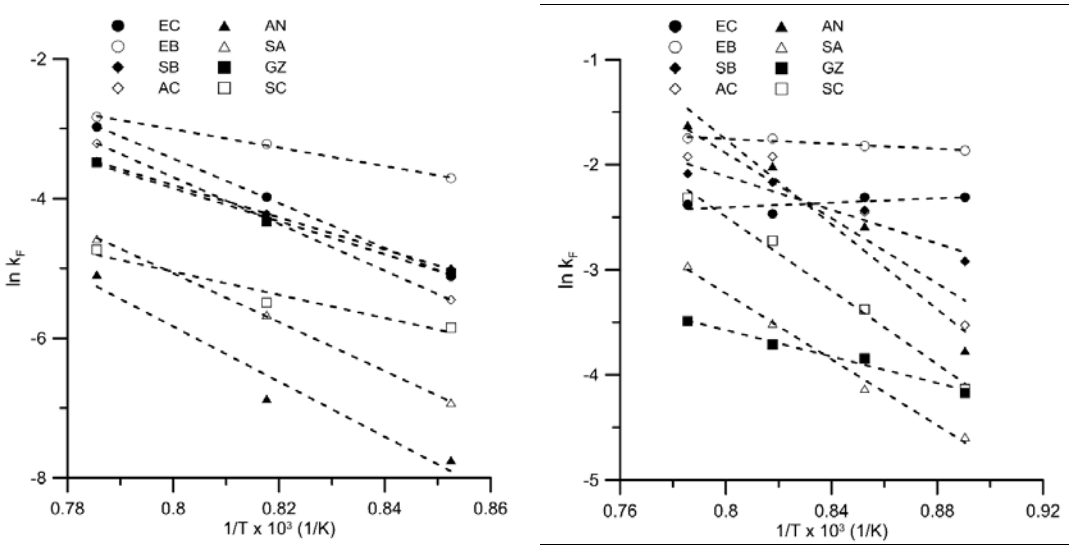

Figure 26: The Arrhenius plots for reactants CH_4 in Figure 26a and CO in Figure 26b. For CH_4 (a), the effective rate constant (k_F) was calculated at ω=0.999 (SA ω=0.9995, AN ω=0.9998) and for CO (b) at ω=0.99.

3.1.6 Effect of heat treatment

A study was undertaken to investigate the effect of heat treatment on the manganese ores performance, see Paper VI. There are several reasons why such a study was undertaken, including the possibility of significant phase changes during heat-up which may affect the particles physically and chemically. This has previously been seen for a number of natural materials and

could have implications for a real CLC unit. This is why a lot of oxygen carriers based on ores are heat treated prior to use[78,91,92]. Further, literature data suggests that there may be major changes in reactivity between heat-treated ores and fresh ones[93]. Based on these results and the difficulties seen in pilot operation with natural fresh materials, it was decide to pursue an experimental endeavor of establishing the effect of heat treatment of manganese ores. The aim of this study is thus to investigate how heat treatment of manganese ores affect its reactivity and fluidizability during the redox reactions occurring in CLC. The possible transformations during calcination/heat-up was also investigated.

Figure 27 shows temperature ramping using air in a TGA for two manganese ores, TS and NCH. Here, the heat treated and untreated samples of the respective ore are compared. It is quite clear that major mass losses are possible during heating, adding up to almost 17 wt% for the fresh TS material. It can be seen that for the untreated Tshipi ore there is an initial slow weight decrease that become more rapid as the temperature exceeds 600°C. At around the same temperature there is CO_2 released from the ores, see Paper VI. These are likely decomposition of $CaCO_3$ or $CaMn(CO_3)_2$. Depending upon the ore, mass losses can also be explained by release of oxygen gas, due to decomposition of, for instance, MnO_2. This large weight decrease is not be seen for the heat treated samples, the exception being the NCH ore. There is a small weight increase as the temperature is lowered which is because the ores oxidizes to other forms, such as Mn_2O_3.

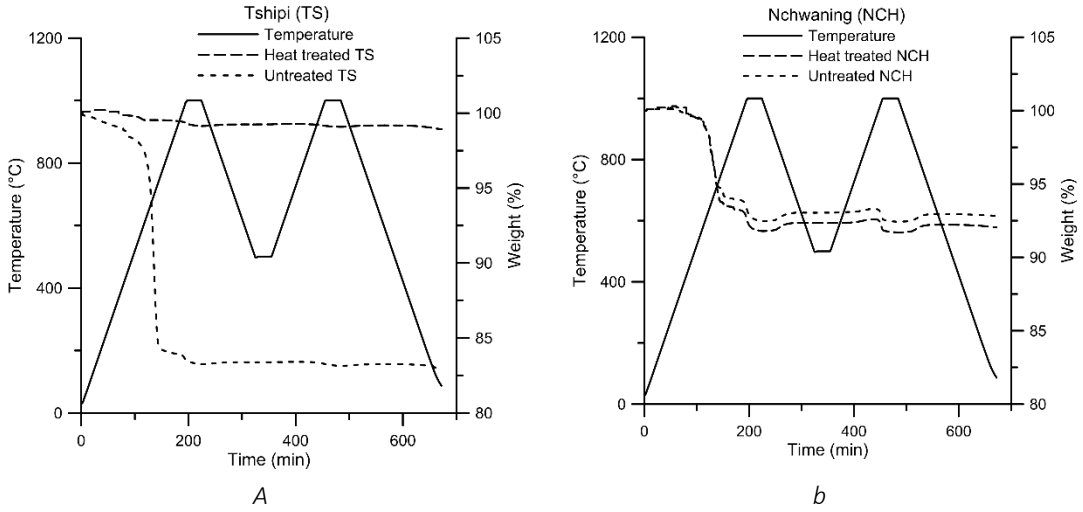

Figure 27: TGA experiments comparing the untreated and heat treated particles of each ore. Tshipi (a), Nchwaning (b).

Figure 28 shows a comparison of the CO_2 yield for methane between heat-treated manganese ore and untreated manganese ore as obtained in the batch fluidized bed at 950°C. The figure shows how the reactivity changes over many cycles. There seems to be a general trend of decreasing reactivity after the first cycles, followed by relatively stable behavior, the exception being BR, where the reactivity clearly decreases as a function of cycle. The thermal treatment seems to have some effect for the ores with highest reactivity. Both Buritirama and Tshipi have slightly higher reactivity in the heat-treated state compared to the untreated. The difference can largely be explained by the mass-losses during heat-up, meaning that the amount of active oxygen carrier is less for the untreated ores. However, it is the other way around for Sibelco Braunite and Nchwaning, where the untreated ore shows somewhat higher reactivity than the heat treated ones. The ores were also investigated with regards to reactivity with syngas, see Paper VI. The reactivity with syngas was less stable than what was seen for methane, however the general trend

between heat treated and untreated was also seen with syngas. With respect to fluidizability, no ores defluidized during heat-up or during redox cycling with methane. However, Buritirama defluidized during the reduction with syngas at 950°C. This happened with both the calcined and untreated samples, and could possibly be explained by interactions with the sand which was used as part of the bed material.

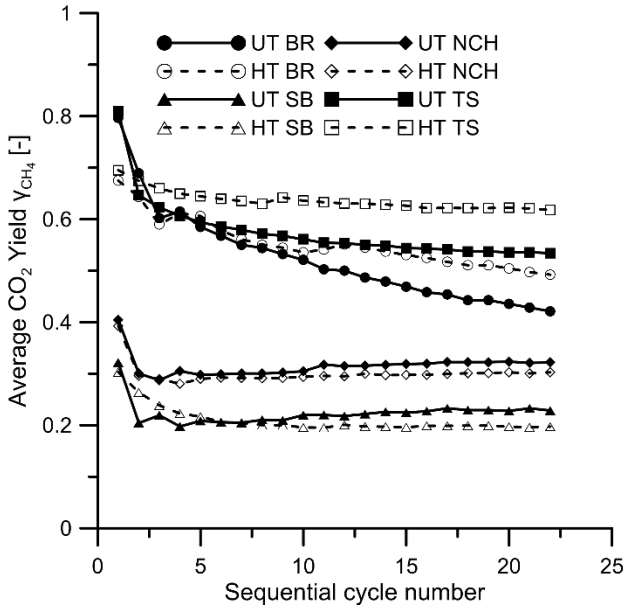

Figure 28: Methane conversion at 950°C over 21 redox cycles. Data is shown for four different ores, both heat treated (HT) and untreated (UT).

3.2 Manganese ores in the circulating fluidized system

The experiments in the batch reactor give an indication of reactivity of the ores, but only a limited number of cycles is possible. Thus as part of the general endeavor to evaluate the applicability of manganese ores, experiments were also conducted with several materials using a continuous circulating reactor, where the ores are exposed to many cycles at relevant conditions. The materials were chosen based on their composition, as mentioned in Section 2.3.2. In this thesis, the results of oxygen uncoupling and reactivity with methane and syngas will be discussed. For results with biomass volatiles, the reader is referred to Paper V.

3.2.1 Oxygen Release

The oxygen release properties for the ores were investigated in the bench-scale 300 W circulating fluidized system[26,77,94]. This was done to determine if the oxygen release properties were stable under continuous operation.

Figure 29 shows the oxygen concentration from the fuel reactor at different temperatures for all investigated ores. During the tests, the oxygen concentration was measured in both air and fuel reactor. In the air reactor the oxygen concentration was 19.5-21%, which was similar for all of the ores. This concentration of oxygen is significantly higher than that in any of the batch reactor experiments and likely has an effect on what phases are present and the resulting oxygen release from the decomposition of these phases.

The range of oxygen release is wide but all ores used released oxygen during continuous operation, which confirms the results seen from the screening in the batch unit, Section 3.1.1. Similar to the batch reactor results with respect to oxygen uncoupling, the oxygen release rates vary over a wide range, with the highest concentrations measured with Tshipiand Gui Zhou. The change in oxygen release over time was not investigated in Paper V. However, no significant change could be seen in fuel conversion in over 30 h of operation in the 300 W unit, which suggest that the oxygen release properties remained stable.

The amount of oxygen released to the gas phase is significantly larger, in terms of volume procent of oxygen, than in the batch experiments, which is reasonable because of the higher ratio of oxygen carrier to gas flow. As such, Tshipi and Gui Zhou respectively released 1 and 3 volume% of O_2 at 900°C. The same was seen in the batch experiments, where Gui Zhou released more oxygen than Tshipi when utilizing inert gas, which would suggest that the results would be comparable despite the quantitative difference. However, Braunite and Elwaleed C had superior oxygen release compared to Tshipi in the batch reactor. In the circulating unit the same relative oxygen release was seen when the material was fresh, i.e. when no fuel had been used. However, the oxygen release seemed to increase for Braunite and Elwaleed C after the ores had been used with fuel, thus reaching similar oxygen release rate as fresh Gui Zhou.

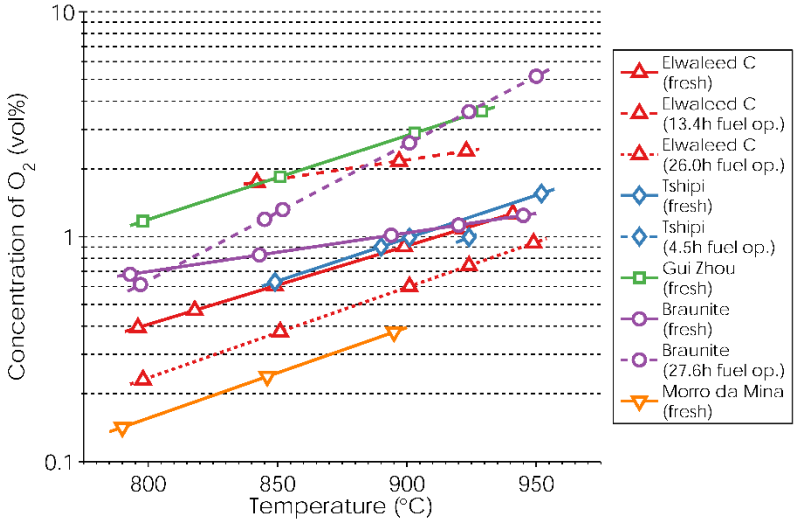

Figure 29: Oxygen release for all examined ores at different temperatures. The ores were tested in both heat-treated state and used state, i.e. after a period of fuel operation (Taken from Paper V).

3.2.2 Syngas

The conversion of syngas was investigated for Elwaleed C, Tshipi, Gui Zhou, and Braunite, Morro da Mina was not tested with either syngas or methane as it turned to dust during experiments with biomass volatiles. Figure 30 shows the CO_2 yield at varied specific fuel-reactor bed mass at different fuel reactor temperatures using syngas as fuel. During the experiments with syngas, the CO_2 yield was never below 80% for any of the materials at any of the tested conditions. The highest CO_2 yield achieved was 98% with Braunite using 371 kg/MWth at 900°C. Although it achieved the highest conversion it generally had lower reactivity towards syngas than the other ores, meaning that it required higher bed mass relative to fuel input to achieve the same degree of conversion. In general, the relative reactivity, order from highest to lowest, was similar to the batch reactor

results, e.g. Figure 21. Here, Tshipi had the best reactivity, followed by Elwaleed C, Braunite, and Gui Zhou. From Figure 30, the latter seems to have a higher relative reactivity in the continuous unit.

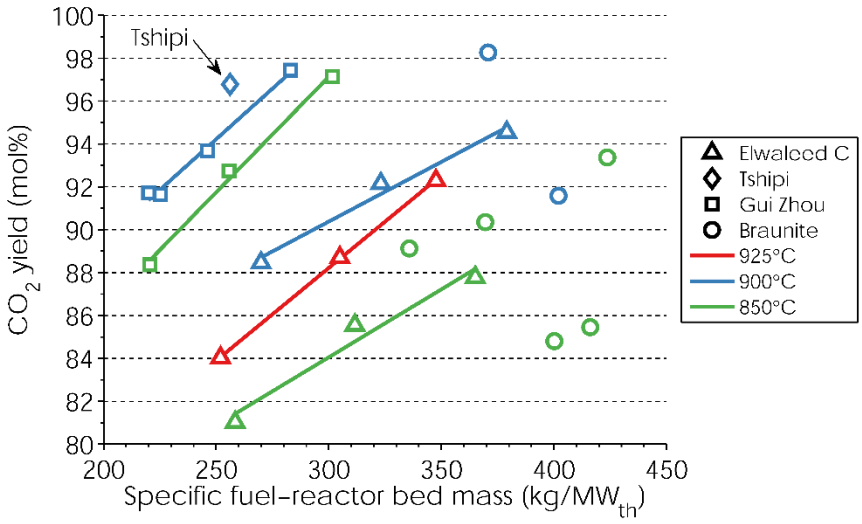

Figure 30: CO_2 yield at varied specific fuel-reactor bed mass at different fuel reactor temperatures with syngas as fuel. The results for Gui Zhou and Elwaleed grade C are shown with fitted lines (Taken from Paper V).

3.2.3 Methane

The conversion of methane was investigated for Elwaleed C, Gui Zhou, and Braunite. Figure 31 shows the CO_2 yield at varied specific fuel-reactor bed mass at different fuel reactor temperatures using methane as fuel. It can be seen that Gui Zhou clearly has a higher reactivity towards methane than Elwaleed C and Braunite, despite the fact that both of them have somewhat higher reactivity towards methane than Gui Zhou in the batch system, see Figure 18b. It is possible that there is inferior mixing between oxygen carrier and fuel in the 300 W and that Gui Zhou´s high oxygen release capabilities help mitigate the mixing problem, allowing gaseous oxygen to meet the fuel in, for instance, the freeboard.

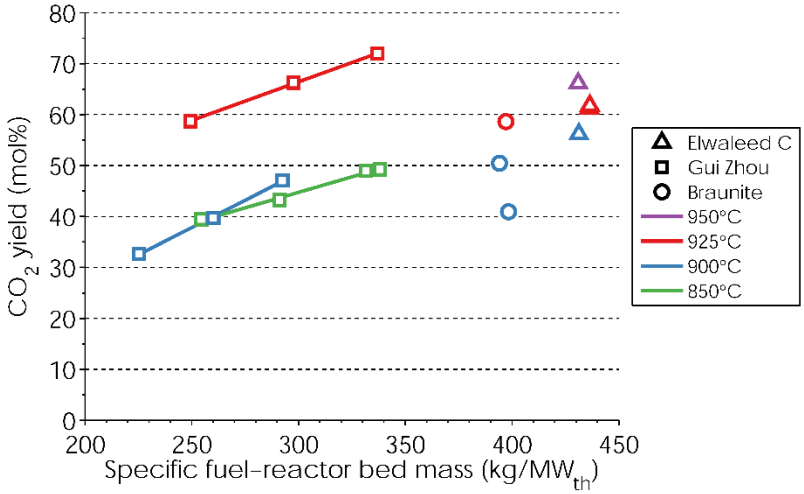

Figure 31: CO_2 yield at varied specific fuel-reactor bed mass at different fuel reactor temperatures with methane as fuel. The results for Gui Zhou are shown with fitted lines. Tshipi was not tested with methane. (Taken from Paper V).

3.3 Phase Characterization

3.3.1 XRD

Phase characterization was performed using x-ray powder diffraction (XRD). The characterization was performed on the particles at different stages, i.e. fresh, heat treated and used, i.e. after the cycling in the batch and continuous units. The detailed results are given in the attached papers. Figure 32 shows XRD spectra of the Tshipi ore at different stages, including fresh (untreated), heat treated and used (material previously used in the batch reactor). In paper VI, Tshipi was shown to release CO_2 during heat up and from Figure 32a it can be seen that there are phases such as calcite ($CaCO_3$) and kutnohorite ($Ca(Mn,Mg)(CO_3)_2$) which could decompose and release CO_2. When comparing the fresh materials in either Figure 32a or Figure 32b it can be seen that braunite I can only be found in the fresh sample. However braunite II seems to be more stable as it was found in both fresh and used sample in the untreated material in Figure 32a. There seems to be formation of the perovskite $CaMnO_3$ during heating, and it was found in all TS samples except untreated fresh material. The perovskite calcium manganite, $CaMnO_3$, is a highly promising oxygen carrier with CLOU properties[47–49], and it is very much possible that this phase is active during the uncoupling of oxygen seen in Figure 14. $CaMnO_3$ was also found in both Gloria and Slovakian ore.

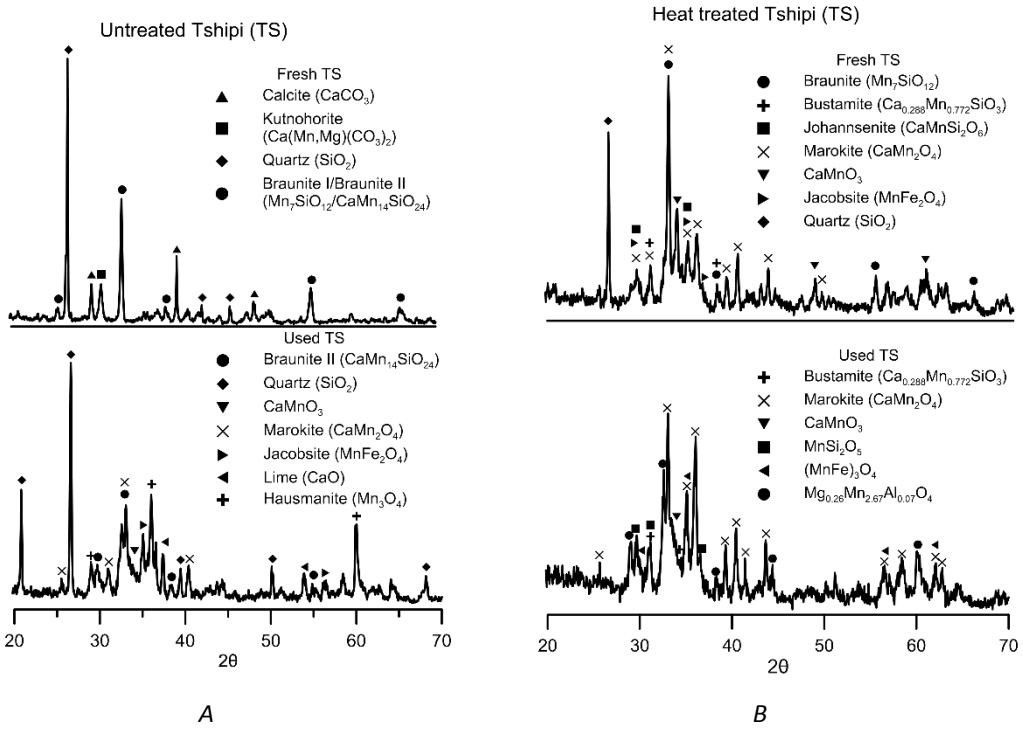

Figure 32: Characterization of the Tshipi manganese ore with XRD. The untreated particles, both fresh and used, are shown in a and the heat treated in b.

It should be noted that phase identification was often difficult due to poor peak separation. This means that the phases listed in Table 8 are likely present, but additional phases might exist as well. Phases that were common in the ores were $(Mn,Fe)_2O_3$ (bixbyite), $(Mn,Fe)_3O_4$, Fe_3O_4 and SiO_2. Si is present in the ores both as braunite (Mn_7SiO_{12}) and SiO_2 phases. However the braunite phase seems to decompose during the experiment. In Paper III a thermodynamic evaluation was made based on the Mn-Fe-Si-O system, and it was seen that at prevailing CLC conditions the most likely phases were braunite and bixbyite, depending on the actual composition. Still, as is evident from Table 8, the most relevant phase seems to be bixbyite. Still, the chemistry is very complex, and

identification not always totally clear, meaning that phases such as braunite could still be active. In fact, from the thermodynamic analysis in Paper III, it can be speculated that braunite is active for CLOU in many of the Mn-rich oxygen carriers. This is simply because bixbyite will not form at higher temperatures, see Figure 4. On the other hand, the Mn-Si system is still active at these conditions, see Figure 5.

Table 8: Phases in the manganese ores identified with XRD. The ores used were taken from the experiments in the batch reactor with CH_4 and were oxidized and cooled in 5% O_2.

Ores	Identified phases				
EB (Fresh)	$(Mn,Fe)_2O_3$	Fe_2O_3	MnO_2		
EB (Used)	$(Mn,Fe)_2O_3$	$(Mn,Fe)_3O_4$	Fe_2O_3		
EC (Fresh)	$(Mn,Fe)_2O_3$	$(Mn,Fe)_3O_4$	Fe_2O_3	Fe_3O_4	
EC (Used)	$(Mn,Fe)_2O_3$	$(Mn,Fe)_3O_4$	SiO_2		
AN (Fresh)	Mn_3O_4	Fe_3O_4	$(Mn,Fe)_3O_4$		
AN (Used)	$(Mn,Fe)_3O_4$	Fe_2O_3	SiO_2		
AC (Fresh)	$(Mn,Fe)_3O_4$	Fe_3O_4	$CaMn_2O_4$	SiO_2	Mn_7SiO_{12}
AC (Used)	$(Mn,Fe)_3O_4$	Fe_3O_4	$CaMn_2O_4$	SiO_2	
SA (Fresh)	$(Mn,Fe)_2O_3$	$(Mn,Fe)_3O_4$	Mn_7SiO_{12}	SiO_2	
SA (Used)	$(Mn,Fe)_2O_3$	$(Mn,Fe)_3O_4$	Fe_2O_3	Mn_3O_4	
GZ (Fresh)	$(Mn,Fe)_2O_3$	Fe_2O_3	Mn_2O_3		
GZ (Used)	$(Mn,Fe)_2O_3$	$(Mn,Fe)_3O_4$	Fe_2O_3	Mn_2O_3	
SC (Fresh)	$(Mn,Fe)_2O_3$	Fe_3O_4	Mn_7SiO_{12}	SiO_2	Mn_3O_4
SC (Used)	$(Mn,Fe)_2O_3$	Mn_3O_4	Fe_2O_3	SiO_2	

3.3.2 SEM-EDX

In order to obtain more information on the composition of the particles, additional analyses were done with SEM-EDX (Scanning electron microscope – energy dispersive x-ray spectroscopy). A number of the fresh ores (only heat treated) were cast in epoxy and then polished to expose the cross section inside the particles. A large number of particles in the ores were mapped with respect to elemental composition. The EDX results for Tshipi are shown in Figure 33. It can be seen that there are a few particles containing mostly Si, with very small quantities of other elements, including Mn. Thus, this is likely SiO_2. Manganese seem to mostly be associated with calcium, which is not totally unexpected, as these are the two main elements in this ore, see Table 2. The manganese phase present could be $CaMnO_3$ or $CaMn_2O_4$, both of which have been identified with XRD, see Figure 32. In addition, braunite was found with the XRD, but no particles were identified with Mn and Si associated to a large extent.

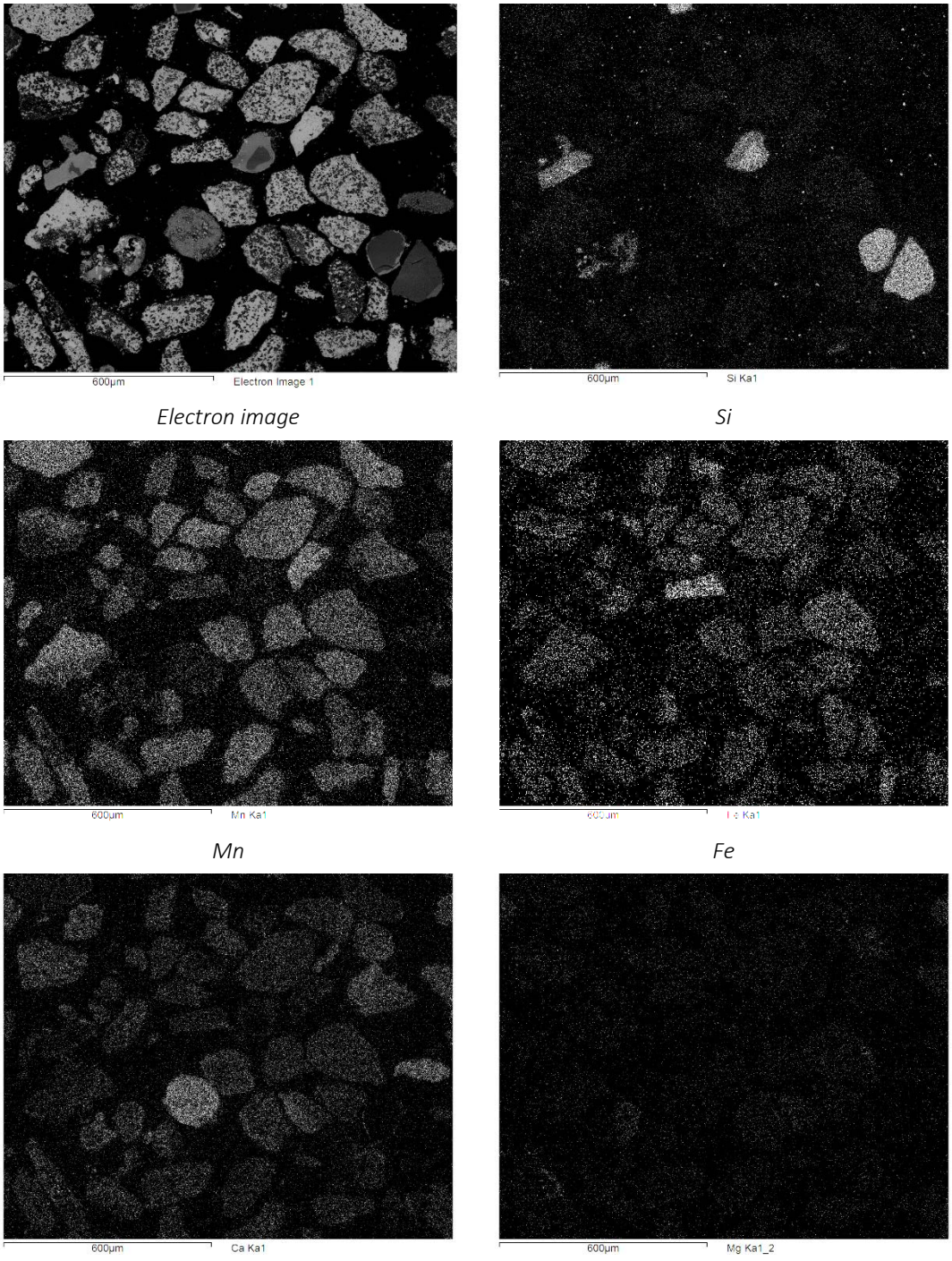

Electron image *Si*

Mn *Fe*

Ca *Mg*

Figure 33: SEM-EDX maps displaying the distribution of elements in Tshipi manganese ore.

Figure 34 show the distribution of elements in Metmin manganese ore. This is an ore with totally different elemental composition than the Tshipi ore, see Table 2. It can be seen that Si is present to a large extent in particles separate from Mn and Fe. The Mn and Fe correlate to each other to a large degree, confirming the presence of bixbyite. Metmin, being an iron-rich ore, has excess iron not correlated to manganese, and this is clearly seen in the mapping.

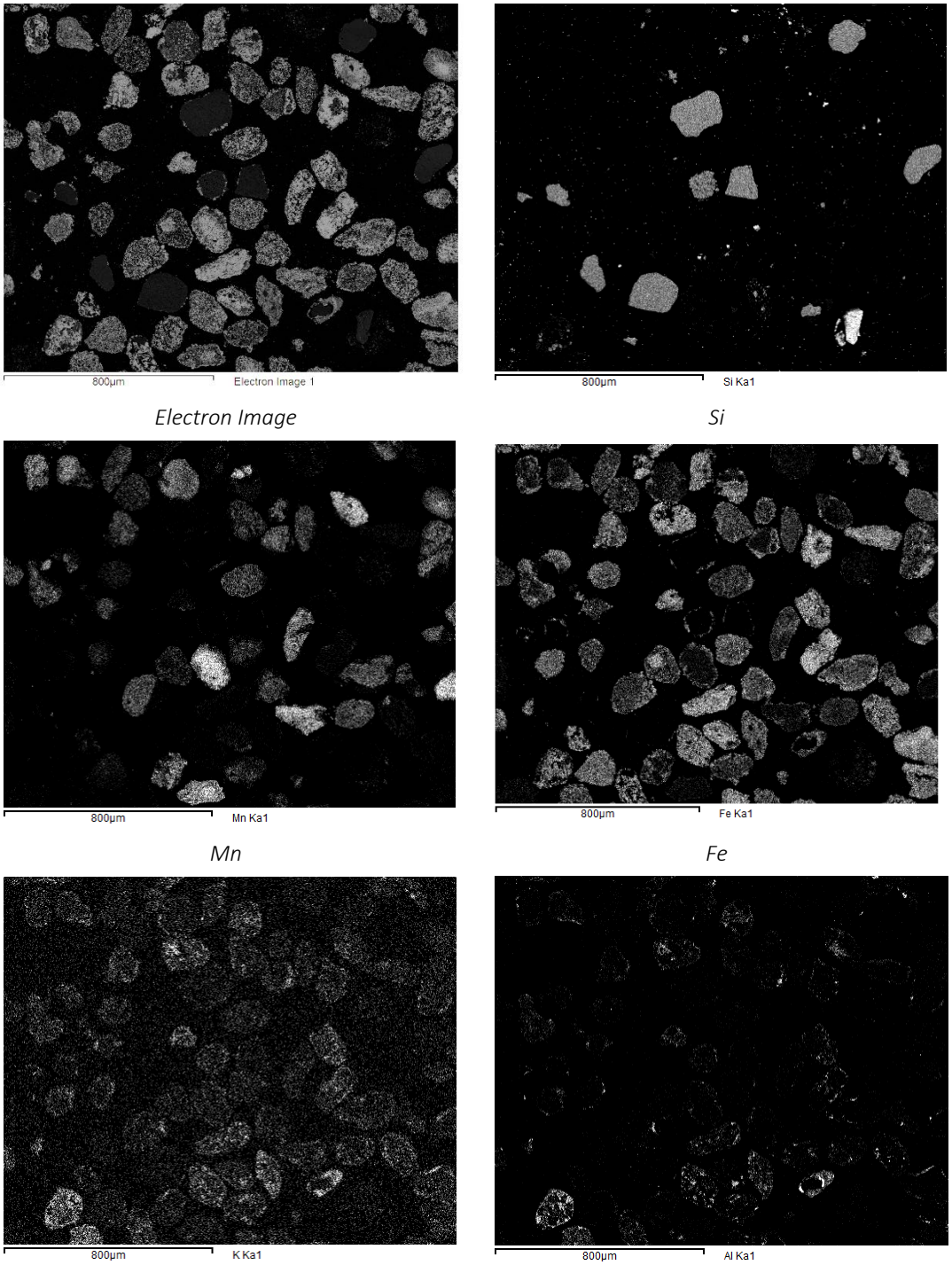

Figure 34: SEM-EDX maps displaying the distribution of elements in Metmin manganese ore.

3.3.3 Physical Properties

Table 9 lists the results for the attrition tests, as well as the properties of the ores such as crushing strength and BET surface area. The particles that were tested had all been heat treated, as stated in Section 2.1.1 For the attrition test in the jet-cup rig, the tested particles had been tested with methane according to the procedure in Table 4. BET analysis was done on both unused particles (Fresh) and particles previously used in the batch reactor with methane (Used), see Section 2.2.2.2.

It is clear that there has been a decrease in surface area for all ores, which indicates a change in the structure during testing, including possible changes in the porosity. The most dramatic decrease was seen for the EB ore, where the specific surface area decreased from 16.4 to 0.6 m^2/g during the experiments. It is possible that these structural changes are the reason for the decrease in reactivity seen for syngas and methane following cycles at higher temperatures, see Figure 19, although this depends very much on the rate limiting reaction step during reaction.

The attrition of the ores investigated in the batch as determined in the jet cup test rig vary between 1.2 to 8.4 wt%/h shown in Table 9. This should be compared to the benchmark oxygen carrier ilmenite, which has an attrition index of 5.7 wt%/h[88].

In Figure 35a and Figure 35b the attrition index is compared to the average CO_2 yield from CH_4 and CO, respectively. There may be a general correlation between the attrition index and the reactivity, with more reactive ores showing less resistance towards attrition. However, there is a wide spread between the data points, suggesting that there is no statistical significant correlation between the attrition index and reactivity for the available data. However, there are several ores which have a combination of low attrition (<2 wt%/h) and reasonable reactivity both with syngas and methane.

Of all ores tested in the continuous CLC unit, Guizhou ore exhibited the most stable fuel conversion properties over the entire test campaign as well as the most stable particle characteristics, see Paper V. In total, the materials were run for 7-32 h with fuel (roughly 80-280 redox cycles) and considerably longer under hot conditions with inert gas or air as fluidizing medium. Attrition and fine production, as observed in the 300 W unit, varied between 0.05 wt%/h (Guizhou ore) and 1.2 wt%/h (Tshipi ore). The attrition index, as measured in the jet-cup are similar for these materials, although somewhat higher for Tshipi.

Table 9: Results from the material characterization

Mn Ore	**EG**	**SL**	**MT**	**NCH**	**GL**	**BR**	**SAA**	**UMK**	**SAB**	**TS**
Attrition Index (wt%/h)	4.6	4.3	6.1	2.4	4.3	2.8	2.2	4.9	2.4	3.2
Crushing Strength, N	3.7	3.7	1.8	3.8	4.5	1.9	4.3	4.2	4.7	2.6
BET Fresh (m^2/g)	0.75	6.1	1.2	0.86	1.1	1.2	1.2	12	0.41	0.7
BET Used (m^2/g)	0.38	0.78	0.71	0.32	0.49	0.27	0.42	0.81	0.23	0.47
Mn Ore	**EC**	**EB**	**SB**	**AC**	**AN**	**SA**	**GZ**	**SC**	**HM**	**Ilmenite**
Attrition Index (wt% /h)	4.07	3.59	1.29	4.51	1.99	1.21	2.88	1.37	8.4	5.7[88]
Crushing Strength (N)	1.7	1.9	3.2	2.2	2.8	3.4	2.4	3.2	2	-
BET Fresh (m^2/g)	0.39	16.4	0.28	0.61	0.14	0.11	1.46	0.1	1.4	-
BET Used (m^2/g)	0.5	0.58	0.22	0.48	0.18	0.13	0.64	0.13	0.63	-

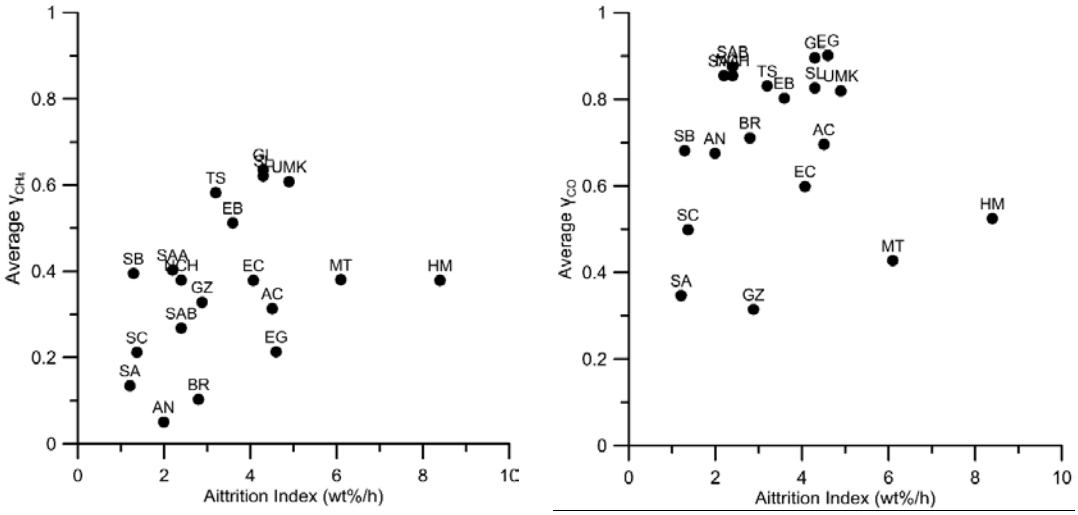

a *b*

Figure 35: Comparison between the attrition index and the average CO_2 yields as obtained in the batch fluidized bed for CH_4 in Figure 35a and CO in Figure 35b

4 Discussion

This work is the first comprehensive study of manganese ores as oxygen carriers in chemical looping combustion. Through analysis of almost twenty different ores with a number of analysis tools, it has been shown that manganese ores could be very promising oxygen carriers for chemical-looping combustion. It has clearly been demonstrated that all of the tested manganese ores released oxygen to the gas phase through chemical-looping with oxygen uncoupling (CLOU). The effect is likely due to the presence of so-called combined manganese oxides, some which have been identified in this work. The rate of the CLOU effect was small for most ores in nitrogen gas, but could be increased dramatically when char was introduced to the bed, with some ores having up to 1 wt% oxygen capacity for CLOU, see Figure 15. Still, the rate of release is small compared to many synthetic particles, such as CuO[95] or $(Mn,Fe)_2O_3$[42]. This means that it probably cannot be expected that uncoupled oxygen can convert fuel entirely through combustion, but that rather parallel CLC and CLOU mechanisms will be active. Still, the CLOU effect could be very important in compensating for inferior gas-solid mixing in a fluidized bed, and also be important in regards to converting fuel components in the freeboard. It has been seen that the volatile contact with oxygen carrier particles could be low due to plume formation. Further, in a well-mixed fluidized bed of oxygen carrier and char particles, it is also expected that fuel gas intermediates will be generated on top of the bed, and these will also have limited contact with oxygen carrier particles[96]. However the gaseous oxygen released through CLOU could promote burnout in the freeboard.

The reactivity of the manganese ores was good, achieving close to 80% CO_2 yields with methane and 95% with CO at 1000°C and using specific solids inventories of 57 kg/MW and 25 kg/MW respectively. However the reactivity varied greatly among the ores and it was found that the highest CO_2 yields was achieved with high Ca-containing manganese ores, although this was not always the case. It is possible that $CaMnO_3$ is one of the active phases for CLOU, and was confirmed to be present in two ores, TS and GL, which both had high uncoupling activity, see Figure 16. These ores had low Fe-content and as such unlikely to have a significant presence of bixbyite with high Fe in the ore, the only possible phase to be oxidized at temperatures above 850°C, see Figure 4.

As the span in reactivity of manganese is great there are ores that have quite poor reactivity. It may be possible to enhance the reactivity through copper impregnation[72,73]. Only a few wt% of copper may be required to get a significant increase in reactivity[72,73]. Another option is to produce $CaMnO_3$ with manganese ore and CaO or $Ca(OH)_2$[71] which would likely lead to an increase in reactivity but a vulnerability to sulphur, see Paper I. The benefit of such methods is of course to be able to utilize the entire range of manganese ores and deposits, many which likely can be obtained at low cost[97].

5 Conclusions

In this work around twenty different manganese ores have been evaluated as oxygen carriers for CLC and CLOU. The materials have been evaluated and characterized with a number of methods, most importantly their reactivity with methane and syngas in batch and continuous units. In addition, their propensity to release gaseous oxygen through CLOU has been determined. Some of the main conclusions of this work are:

- There was oxygen release to the gas phase from all ores at high temperatures, thus confirming the presence of combined Mn-oxides in all materials. In nitrogen, the highest release rate was from ores with a high Fe/Mn ratio. However, with char added to the bed the ores with significant Ca were the most reactive.
- The reactivity of the ores varied in a wide range, depending upon ore, fuel, degree of reduction, and temperature. Nevertheless, the ores had a relatively stable performance as a function of cycle.
- It is likely that different combined Mn-oxides are active during the reduction process, and depends upon the ore type and composition. Some identified phases including bixbyite, braunite and calcium manganite. More specifically, Mn_7SiO_{12}, $(Mn,Fe)_2O_3$, $CaMn_2O_4$ and $CaMnO_3$ have been identified in the heat treated and used ores.
- Some ores exhibit major mass loss upon heating, mainly due to calcination of carbonates and decomposition of unstable oxides.
- A small difference in reactivity could be seen between heat treated and untreated ores, which may be attributed to less amount of active material in the bed.
- The experiments in the continuous unit confirms that some ores have a combination of high reactivity with fuel gases and moderate stability for long periods of time.
- The relative reactivity of the ores between batch and circulating unit was similar, with some minor differences. These may be explained by a number of factors, including the gas-solid contact and variable inventory of particles in the fuel reactor.
- As manganese ores are abundant and currently cheap, they could be highly applicable for use with CLC, especially when employing solid fuels.

6 References

1. Eickemeier, P.,Schlömer, S.,Farahani, E.,Kadner, S.,Brunner, S.,Baum, I. & Kriemann, B. Climate Change 2014 Mitigation of Climate Change Working Group III Contribution to the Fifth Assessment Report of the Intergovernmental Panel on Climate Change. *Cambridge Univ. Press* (2014).
2. Lenton, T. M. Early warning of climate tipping points. *Nat. Clim. Chang.* **1,** 201–209 (2011).
3. International Energy Agency. *Report on: Energy technology perspectives: scenarios and strategies to 2050.* (2013).
4. Metz, B.,Davidson, O.,Coninck, H. de,Loos, M. & (eds.), L. M. IPCC special report on carbon dioxide capture and storage. *Cambridge Univ. Press* (2005).
5. Kovscek, A. R. & Cakici, M. D. Geologic storage of carbon dioxide and enhanced oil recovery . II . Cooptimization of storage and recovery. *Energy Convers. Manag.* **46,** 1941–1956 (2005).
6. Freund, P. & Ormerod, W. G. Progress towards storage of carbon dioxide. *Energy Convers. Manag.* **38,** 199–204 (1997).
7. Cooper, C. A technical basis for carbon dioxide storage. *Energy Procedia* **1,** 1727–1733 (2009).
8. Azar, C.,Johansson, D. J. A. & Mattsson, N. Meeting global temperature targets — the role of bioenergy with carbon capture and storage. *Environ. Res. Lett.* **8,** (2013).
9. Azar, C.,Lindgren, K.,Obersteiner, M.,Riahi, K.,Vuuren, D. P. Van,Elzen, K. M. G. J. Den,Möllersten, K. & Larson, E. D. The feasibility of low CO_2 concentration targets and the role of bio-energy with carbon capture and storage (BECCS). *Clim. Chang.* **100,** 195–202 (2010).
10. Kriegler, E.,Weyant, J. P.,Blanford, G. J.,Krey, V.,Clarke, L.,Edmonds, J.,Fawcett, A.,Luderer, G.,Riahi, K.,Richels, R.,Rose, S. K.,Tavoni, M. & Vuuren, D. P. Van. The role of technology for achieving climate policy objectives : overview of the EMF 27 study on global technology and climate policy strategies. *Clim. Chang.* **123,** 353–367 (2014).
11. Kjärstad, J.,Skagestad, R.,Henrik, N. & Johnsson, F. Transport of CO_2 in the Nordic region. *Energy Procedia* **63,** 2683–2690 (2014).
12. Kjärstad, J.,Skagestad, R.,Henrik, N. & Johnsson, F. Ship transport — A low cost and low risk CO_2 transport option in the Nordic countries. *Int. J. Greenh. Gas Control* **54,** 168–184 (2016).
13. Scholes, C. A.,Smith, K. H.,Kentish, S. E. & Stevens, G. W. International Journal of Greenhouse Gas Control CO 2 capture from pre-combustion processes — Strategies for membrane gas separation. *Int. J. Greenh. Gas Control* **4,** 739–755 (2010).
14. Wang, M.,Lawal, A.,Stephenson, P.,Sidders, J.,Ramshaw, C.,Hill, W.,Park, B. & Sn, S. Chemical Engineering Research and Design Post-combustion CO_2 capture with chemical absorption : A state-of-the-art review. *Chem. Eng. Res. Des.* **89,** 1609–1624 (2010).
15. Cormos, C. & Petrescu, L. Evaluation of calcium looping as carbon capture option for combustion and gasification power plants. *Energy Procedia* **51,** 154–160 (2014).
16. Toftegaard, M. B.,Brix, J.,Jensen, P. A.,Glarborg, P. & Jensen, A. D. Oxy-fuel combustion of solid fuels. *Prog. Energy Combust. Sci.* **36,** 581–625 (2010).
17. Mukherjee, S.,Kumar, P.,Yang, A. & Fennell, P. Journal of Environmental Chemical Engineering Energy and exergy analysis of chemical looping combustion technology and

comparison with pre-combustion and oxy-fuel combustion technologies for CO_2 capture. *J. Environ. Chem. Eng.* **3,** 2104–2114 (2015).

18. Lyngfelt, A. & Leckner, B. A 1000 MWth boiler for chemical-looping combustion of solid fuels – Discussion of design and costs. *Appl. Energy* **157,** 475–487 (2015).
19. Abanades, J. C.,Arias, B.,Lyngfelt, A.,Mattisson, T.,Wiley, D. E.,Li, H.,Ho, M. T.,Mangano, E. & Brandani, S. Emerging CO_2 capture systems. *Int. J. Greenh. Gas Control* **40,** 126–166 (2015).
20. Moldenhauer, P.,Rydén, M.,Mattisson, T. & Lyngfelt, A. Chemical-looping combustion and chemical-looping reforming of kerosene in a circulating fluidized-bed 300 W laboratory reactor. *Int. J. Greenh. Gas Control* **9,** 1–9 (2012).
21. Adánez, J.,Abad, A.,Garcia-labiano, F.,Gayán, P. & Diego, L. F. De. Progress in Chemical-Looping Combustion and Reforming technologies. *Prog. Energy Combust. Sci.* **38,** 215–282 (2012).
22. Ohlemüller, P.,Busch, J.-P.,Reitz, M.,Ströhle, J. & Epple, B. Chemical-Looping Combustion of Hard Coal: Autothermal Operation of a 1 MW_{th} Pilot Plant. *J. Energy Resour. Technol.* **138,** 42203 (2016).
23. Huijun, G.,Laihong, S.,Fei, F. & Shouxi, J. Experiments on biomass gasification using chemical looping with nickel-based oxygen carrier in a 25 kWth reactor. *Appl. Therm. Eng.* **85,** 52–60 (2015).
24. Mattisson, T.,Lyngfelt, A. & Leion, H. Chemical-looping with oxygen uncoupling for combustion of solid fuels. *Int. J. Greenh. Gas Control* **3,** 11–19 (2009).
25. Hallberg, P.,Jing, D.,Rydén, M.,Mattisson, T. & Lyngfelt, A. Chemical Looping Combustion and Chemical Looping with Oxygen Uncoupling Experiments in a Batch Reactor Using Spray-Dried $CaMn_{1-x}M_xO_{3-\delta}$ (M = Ti, Fe, Mg) Particles as Oxygen Carriers. *Energy & Fuels* **27,** 1473–1481 (2013).
26. Källén, M.,Rydén, M.,Mattisson, T. & Lyngfelt, A. Operation with combined oxides of manganese and silica as oxygen carriers in a 300 W th chemical-looping combustion unit. *Energy Procedia* **63,** 131–139 (2014).
27. Moldenhauer, P.,Rydén, M.,Mattisson, T.,Hoteit, A.,Jamal, A. & Lyngfelt, A. Chemical-Looping Combustion with Fuel Oil in a 10 kW Pilot Plant. *Energy & Fuels* **28,** 5978–5987 (2014).
28. Moldenhauer, P.,Rydén, M.,Mattisson, T.,Jamal, A. & Lyngfelt, A. Chemical-looping combustion with heavy liquid fuels in a 10 kW pilot plant. *Fuel Process. Technol.* **156,** 124–137 (2017).
29. Hanning, M.,Frick, V.,Mattisson, T.,Rydén, M. & Lyngfelt, A. Performance of Combined Manganese-Silicon Oxygen Carriers and Effects of Including Titanium. *Energy & Fuels* **30,** 1171–1182 (2016).
30. Mattisson, T. Materials for Chemical-Looping with Oxygen Uncoupling. *Hindawi Publ. Corp.* **526375,** (2013).
31. Imtiaz, Q.,Hosseini, D. & Müller, C. R. Review of Oxygen Carriers for Chemical Looping with Oxygen Uncoupling (CLOU): Thermodynamics , Material Development , and Synthesis. *Energy Technol.* **1,** 633–647 (2013).
32. Jerndal, E.,Mattisson, T. & Lyngfelt, A. Thermal analysis of chemical-looping combustion. *Chem. Eng. Res. Des.* **84,** 795–806 (2006).
33. Hossain, M. M. & Lasa, H. I. De. Chemical-looping combustion (CLC) for inherent CO_2 separations — a review. *Chem. Eng. Sci.* **63,** (2008).

34. Lyngfelt, A.,Leckner, B. & Mattisson, T. A uidized-bed combustion process with inherent CO_2 separation ; application of chemical-looping combustion. *Chem. Eng. Sci.* **56,** 3101–3113 (2001).

35. Abad, A.,Mattisson, T.,Lyngfelt, A. & Johansson, M. The use of iron oxide as oxygen carrier in a chemical-looping reactor. *Fuel* **86,** 1021–1035 (2007).

36. Lyngfelt, A. Oxygen Carriers for Chemical Looping Combustion - 4000 h of Operational Experience. *Oil Gas Sci. Technol.* **66,** 161–172 (2011).

37. Adánez-rubio, I.,Abad, A.,Gayán, P.,Diego, L. F. De,García-labiano, F. & Adánez, J. Identification of operational regions in the Chemical-Looping with Oxygen Uncoupling (CLOU) process with a Cu-based oxygen carrier. *Fuel* **102,** 634–645 (2012).

38. Chuang, S. Y.,Dennis, J. S.,Hayhurst, A. N. & Scott, S. A. Development and performance of Cu-based oxygen carriers for chemical-looping combustion. *Combust. Flame* **154,** 109–121 (2008).

39. Mattisson, T.,Leion, H. & Lyngfelt, A. Chemical-looping with oxygen uncoupling using CuO/ZrO_2 with petroleum coke. *Fuel* **88,** 683–690 (2009).

40. Zafar, Q.,Abad, A.,Mattisson, T.,Gevert, B. & Strand, M. Reduction and oxidation kinetics of $Mn_3O_4/Mg–ZrO_2$ oxygen carrier particles for chemical-looping combustion. *Chem. Eng. Res. Des.* **62,** 6556–6567 (2007).

41. Shulman, A.,Cleverstam, E.,Mattisson, T. & Lyngfelt, A. Manganese/iron, manganese/nickel, and manganese/silicon oxides used in chemical-looping with oxygen uncoupling (CLOU) for combustion of methane. *Energy & Fuels* **23,** 5269–5275 (2009).

42. Azimi, G.,Leion, H.,Rydén, M.,Mattisson, T. & Lyngfelt, A. Investigation of different Mn-Fe oxides as oxygen carrier for chemical-looping with oxygen uncoupling (CLOU). *Energy and Fuels* **27,** 367–377 (2013).

43. Azimi, G.,Mattisson, T.,Leion, H.,Rydén, M. & Lyngfelt, A. Comprehensive study of Mn-Fe-Al oxygen-carriers for chemical-looping with oxygen uncoupling (CLOU). *Int. J. Greenh. Gas Control* **34,** 12–24 (2015).

44. Frick, V.,Arjmand, M.,Rydén, M.,Leion, H.,Mattisson, T. & Lyngfelt, A. Screening of combined Mn-Si oxygen carriers for chemical looping with oxygen uncoupling (CLOU). *Energy & Fuels* **29,** 1868–1880 (2015).

45. Rydén, M.,Leion, H.,Mattisson, T. & Lyngfelt, A. Combined oxides as oxygen-carrier material for chemical-looping with oxygen uncoupling. *Appl. Energy* **113,** 1924–1932 (2014).

46. Bakken, E.,Norby, T. & St, S. Nonstoichiometry and reductive decomposition of $CaMnO_{3-\delta}$. *Solid State Ionics* **176,** 217–223 (2005).

47. Rørmark, L.,Wiik, K. & Grande, T. Oxygen stoichiometry and structural properties of $La_{1-x}A_xMnO_{3-\delta}$ (A=Ca or Sr and 0<x<1). *J. Mater. Chem.* **12,** 1058–1067 (2002).

48. Rørmark, L.,Stølen, S.,Wiik, K. & Grande, T. Enthalpies of Formation of $La_{1-x}A_xMnO_{3-\delta}$ (A=Ca and Sr) Measured by High-Temperature Solution Calorimetry. *J. Solid State Chem.* **193,** 186–193 (2002).

49. Leonidova, E. I.,Markov, A. A.,Patrakeev, M. V,Leonidov, I. A. & Kozhevnikov, V. L. Oxygen Nonstoichiometry and the Thermodynamic Properties of Manganites $Ca_{1-x-y}Sr_xLa_yMnO_{3-\delta}$. *Chem. Thermodyn. Thermochem.* **85,** 343–347 (2011).

50. Azimi, G.,Leion, H.,Mattisson, T.,Rydén, M.,Snijkers, F. & Lyngfelt, A. Mn-Fe oxides with support of $MgAl_2O_4$, CeO_2, ZrO_2 and Y_2O_3-ZrO_2 for chemical-looping combustion and chemical-looping with oxygen uncoupling. *Ind. Eng. Chem. Res.* **53,** 10358–10365 (2014).

51. Azimi, G.,Leion, H.,Mattisson, T. & Lyngfelt, A. Chemical-Looping with Oxygen Uncoupling using combined Mn-Fe oxides , testing in batch fluidized bed. *Energy Procedia* **4,** 370–377 (2011).

52. Shulman, A.,Cleverstam, E.,Mattisson, T. & Lyngfelt, A. Chemical - Looping with oxygen uncoupling using Mn/Mg-based oxygen carriers - Oxygen release and reactivity with methane. *Fuel* **90,** 941–950 (2011).

53. Jing, D.,Arjmand, M.,Mattisson, T.,Rydén, M.,Snijkers, F.,Leion, H. & Lyngfelt, A. Examination of oxygen uncoupling behaviour and reactivity towards methane for manganese silicate oxygen carriers in chemical-looping combustion. *Int. J. Greenh. Gas Control* **29,** 70–81 (2014).

54. Arjmand, M.,Frick, V.,Rydén, M.,Leion, H.,Mattisson, T. & Lyngfelt, A. Screening of combined Mn-Fe-Si oxygen carriers for chemical looping with oxygen uncoupling (CLOU). *Energy & Fuels* **29,** 1868–1880 (2015).

55. Mattisson, T.,Jing, D.,Lyngfelt, A. & Rydén, M. Experimental investigation of binary and ternary combined manganese oxides for chemical-looping with oxygen uncoupling (CLOU). *Fuel* **164,** 228–236 (2016).

56. Arjmand, M.,Kooiman, R. F.,Ryde, M.,Leion, H.,Mattisson, T. & Lyngfelt, A. Sulfur Tolerance of $Ca_xMn_{1-y}M_yO_{3-\delta}$ (M=Mg,Ti) Perovskite-Type Oxygen Carriers in Chemical-Looping with Oxygen Uncoupling. *Energy & Fuels* 1312–1324 (2014).

57. Jing, D.,Mattisson, T.,Leion, H.,Rydén, M. & Lyngfelt, A. Examination of perovskite structure $CaMnO_{3-\delta}$ with MgO addition as oxygen carrier for chemical looping with oxygen uncoupling using methane and syngas. *Int. J. Chem. Eng.* **2013,** (2013).

58. Galinsky, N.,Sendi, M.,Bowers, L. & Li, F. $CaMn_{1-x}B_xO_{3-d}$ (B=Al, V, Fe, Co, and Ni) perovskite based oxygen carriers for chemical looping with oxygen uncoupling (CLOU). *Appl. Energy* **174,** 80–87 (2016).

59. Pishahang, M.,Larring, Y.,Sunding, M.,Jacobs, M. & Snijkers, F. Performance of Perovskite-Type Oxides as Oxygen-Carrier Materials for Chemical Looping Combustion in the Presence of H_2 S. *Energy Technol.* **4,** 1305–1316 (2016).

60. Mayer, K.,Penthor, S.,Pröll, T. & Hofbauer, H. The different demands of oxygen carriers on the reactor system of a CLC plant – Results of oxygen carrier testing in a 120 kW th pilot plant. *Appl. Energy* **157,** 323–329 (2015).

61. Rydén, M.,Lyngfelt, A. & Mattisson, T. $CaMn_{0.875}Ti_{0.125}O_3$ as oxygen carrier for chemical-looping with oxygen uncoupling (CLOU)— Experiments in a continuously operating fluidized-bed reactor system. *Int. J. Greenh. Gas Control* **5,** 356–366 (2011).

62. Leion, H.,Larring, Y.,Bakken, E.,Bredesen, R.,Mattisson, T. & Lyngfelt, A. Use of $CaMn_{0.875}Ti_{0.125}O_3$ as Oxygen Carrier in Chemical-Looping with Oxygen Uncoupling. *Energy & Fuels* **23,** 5276–5283 (2009).

63. Jing, D.,Jacobs, M.,Hallberg, P.,Lyngfelt, A. & Mattisson, T. Development of $CaMn_{0.775}Mg_{0.1}Ti_{0.125}O_{3-\delta}$ oxygen carriers produced from different Mn and Ti sources. *Mater. Des.* **89,** 527–542 (2016).

64. Hallberg, P.,Källén, M.,Jing, D.,Snijkers, F.,Noyen, J. Van,Rydén, M. & Lyngfelt, A. Experimental Investigation of $CaMnO_{3-\delta}$ Based Oxygen Carriers Used in Continuous Chemical-Looping Combustion. *Int. J. Chem. Eng.* **2014,** (2014).

65. Hallberg, P.,Hanning, M.,Rydén, M.,Mattisson, T. & Lyngfelt, A. Investigation of a calcium manganite as oxygen carrier during 99 h of operation of chemical-looping combustion in a 10 kW th reactor unit. *Int. J. Greenh. Gas Control* **53,** 222–229 (2016).

66. Fossdal, A.,Bakken, E.,Øye, B. A.,Schøning, C.,Kaus, I.,Mokkelbost, T. & Larring, Y. International Journal of Greenhouse Gas Control Study of inexpensive oxygen carriers for chemical looping combustion. *Int. J. Greenh. Gas Control* **5,** 483–488 (2011).

67. Ksepko, E.,Babinski, P. & Nalbandian, L. The redox reaction kinetics of Sinai ore for chemical looping combustion applications. *Appl. Energy* **190,** 1258–1274 (2017).

68. Mei, D.,Mendiara, T.,Abad, A.,de Diego, L. F.,García-Labiano, F.,Gayán, P.,Adánez, J. & Zhao, H. Evaluation of Manganese Minerals for Chemical Looping Combustion. *Energy & Fuels* **29,** 6605–6615 (2015).

69. Keller, M.,Leion, H. & Mattisson, T. Mechanisms of Solid Fuel Conversion by Chemical-Looping Combustion (CLC) using Manganese Ore: Catalytic Gasification by Potassium Compounds. *Energy Technol.* **1,** 273–282 (2013).

70. Arjmand, M.,Leion, H.,Lyngfelt, A. & Mattisson, T. Use of manganese ore in chemical-looping combustion (CLC)-Effect on steam gasification. *Int. J. Greenh. Gas Control* **8,** 56–60 (2012).

71. Pour, N. M.,Azimi, G.,Leion, H.,Rydén, M. & Lyngfelt, A. Production and examination of oxygen-carrier materials based on manganese ores and $Ca(OH)_2$ in chemical looping with oxygen uncoupling. *AIChE J.* **60,** 645–656 (2014).

72. Xu, L.,Edland, R.,Li, Z.,Leion, H.,Zhao, D. & Cai, N. Cu-Modified Manganese Ore as an Oxygen Carrier for Chemical Looping Combustion. *Energy & Fuels* **28,** 7085–7092 (2014).

73. Xu, L.,Sun, H.,Li, Z. & Cai, N. Experimental study of copper modified manganese ores as oxygen carriers in a dual fluidized bed reactor. *Appl. Energy* **162,** 940–947 (2016).

74. Leion, H.,Mattisson, T. & Lyngfelt, A. Use of Ores and Industrial Products As Oxygen Carriers in Chemical-Looping Combustion. *Energy & Fuels* **23,** 2307–2315 (2009).

75. Frohn, P.,Arjmand, M.,Azimi, G.,Leion, H.,Mattisson, T. & Lyngfelt, A. On the High-Gasification Rate of Brazilian Manganese Ore in Chemical-Looping Combustion (CLC) for Solid Fuels. *AIChE J.* **59,** 4346–4354 (2013).

76. Arjmand, M.,Leion, H.,Mattisson, T. & Lyngfelt, A. Investigation of different manganese ores as oxygen carriers in chemical- looping combustion (CLC) for solid fuels. *Appl. Energy* **113,** 1883–1894 (2014).

77. Rydén, M.,Lyngfelt, A. & Mattisson, T. Combined manganese/iron oxides as oxygen carrier for chemical looping combustion with oxygen uncoupling (CLOU) in a circulating fluidized bed reactor system. *Energy Procedia* **4,** 341–348 (2011).

78. Schmitz, M.,Linderholm, C.,Hallberg, P.,Sundqvist, S. & Lyngfelt, A. Chemical-Looping Combustion of Solid Fuels Using Manganese Ores as Oxygen Carriers. *Energy & Fuels* **30,** 1204–1216 (2016).

79. Linderholm, C.,Schmitz, M.,Knutsson, P. & Lyngfelt, A. Chemical-looping combustion in a 100-kW unit using a mixture of ilmenite and manganese ore as oxygen carrier. *Fuel* **166,** 533–542 (2016).

80. Corathers, L. A. & Machamer, J. F. Industrial minerals & rocks: commodities, markets, and uses. 7th edition. SME. 631–636

81. Dashevskii, V. Y.,Yusfin, Y. S.,Podgorodetskii, G. S. & Baeva, N. V. Production of Manganese Ferroalloys from Usinsk Manganese Ore. **43,** 544–551 (2013).

82. Roberts, R. J.,Irving, E. M. & Simons, F. S. Mineral Deposits of Central America. *Geol. Surv. Bull. United state Gov. Print. Off.* **1034,** (1957).

83. Albuqerque, M. F. do S.,Horbe, M. A. C. & Botelho, N. F. Genesis of manganese deposits in southwestern Amazonia : Mineralogy , geochemistry and paleoenvironment. *Ore Geol. Rev.* **89,** 270–289 (2017).

84. Gutzmer, J.,Beukes, N. J. & Rock, B. Mineral paragenesis of the Kalahari manganese field , South Africa. *Ore Geol. Rev.* **11,** 405–428 (2006).

85. Sorensen, B.,Gaal, S.,Ringdalen, E.,Tangstad, M.,Kononov, R. & Ostrovski, O. Phase compositions of manganese ores and their change in the process of calcination. *Int. J. Miner. Process.* **94,** 101–110 (2010).

86. Kononov, R.,Ostrovski, O. & Ganguly, S. Carbothermal Solid State Reduction of Manganese Ores: 1. Manganese Ore Characterisation. *ISIJ Int.* **49,** 1099–1106 (2009).

87. Post, J. E. Manganese oxide minerals : Crystal structures and economic and enironmental significance. *Proc. Natl. Acad. Sci. U. S. A.* **96,** 3447–3454 (1999).

88. Rydén, M.,Moldenhauer, P.,Lindqvist, S.,Mattisson, T. & Lyngfelt, A. Measuring attrition resistance of oxygen carrier particles for chemical looping combustion with a customized jet cup. *Powder Technol.* **256,** 75–86 (2014).

89. Markström, P.,Linderholm, C. & Lyngfelt, A. Analytical model of gas conversion in a 100kW chemical-looping combustor for solid fuels-Comparison with operational results. *Chem. Eng. Sci.* **96,** 131–141 (2013).

90. Berguerand, N.,Lyngfelt, A.,Mattisson, T. & Markström, P. Chemical Looping Combustion of Solid Fuels in a 10 kW th Unit. *Oil Gas Sci. Technol.* **66,** 181–191 (2011).

91. Adánez, J.,Cuadrat, A.,Abad, A.,Gay, P.,Diego, L. F. De & Garcı, F. Ilmenite Activation during Consecutive Redox Cycles in Chemical-Looping Combustion. *Energy & Fuels* **24,** 1402–1413 (2010).

92. Pröll, T.,Mayer, K.,Bolhàr-nordenkampf, J. & Kolbitsch, P. Natural minerals as oxygen carriers for chemical looping combustion in a dual circulating fluidized bed system. *Energy Procedia* **1,** 27–34 (2009).

93. Schwebel, G. L.,Leion, H. & Krumm, W. Comparison of natural ilmenites as oxygen carriers in chemical-looping combustion and influence of water gas shift reaction on gas composition. *Chem. Eng. Res. Des.* **90,** 1351–1360 (2012).

94. Hanning, M.,Frick, V.,Mattisson, T.,Rydén, M. & Lyngfelt, A. Performance of Combined Manganese − Silicon Oxygen Carriers and Effects of Including Titanium. *Energy & Fuels* **30,** 1171–1182 (2016).

95. Arjmand, M.,Leion, H.,Mattisson, T. & Lyngfelt, A. ZrO_2-Supported CuO Oxygen Carriers for Chemical-Looping with Oxygen Uncoupling (CLOU). *Energy Procedia* **37,** 550–559 (2013).

96. Markström, P.,Linderholm, C. & Lyngfelt, A. Operation of a 100 kW chemical-looping combustor with Mexican petroleum coke and Cerrejón coal. *Appl. Energy* **113,** 1830–1835 (2014).

97. Lyngfelt, A. & Leckner, B. A 1000 MWth boiler for chemical-looping combustion of solid fuels – Discussion of design and costs. *Appl. Energy* **157,** 475–487 (2015).